PTEP

Prog. Theor. Exp. Phys. **2016**, 123D03 (27 pages)
DOI: 10.1093/ptep/ptw166

On the structure observed in the in-flight ^{3}He(K^-, Λp)n reaction at J-PARC

Takayasu Sekihara[1,*], Eulogio Oset[2], and Angels Ramos[3]

[1]*Advanced Science Research Center, Japan Atomic Energy Agency, Shirakata, Tokai, Ibaraki 319-1195, Japan*
[2]*Departamento de Física Teórica and IFIC, Centro Mixto Universidad de Valencia-CSIC, Institutos de Investigación de Paterna, Aptdo. 22085, 46071 Valencia, Spain*
[3]*Departament de Física Quàntica i Astrofísica and Institut de Ciències del Cosmos, Universitat de Barcelona, Martí i Franquès 1, 08028 Barcelona, Spain*
[*]E-mail: sekihara@post.j-parc.jp

Received July 11, 2016; Revised October 7, 2016; Accepted October 15, 2016; Published December 30, 2016

A theoretical investigation is done to clarify the origin of the peak structure observed near the K^-pp threshold in the in-flight ^{3}He(K^-, Λp)n reaction of the J-PARC E15 experiment, which could be a signal of the lightest kaonic nuclei, i.e., the $\bar{K}NN(I = 1/2)$ state. For the investigation, we evaluate the Λp invariant mass spectrum assuming two possible scenarios to interpret the experimental peak. One assumes that the $\Lambda(1405)$ resonance is generated after the emission of an energetic neutron from the absorption of the initial K^-, not forming a bound state with the remaining proton. This uncorrelated $\Lambda(1405)p$ system subsequently decays into the final Λp. The other scenario implies that, after the emission of the energetic neutron, a $\bar{K}NN$ bound state is formed, decaying eventually into a Λp pair. Our results show that the experimental signal observed in the in-flight ^{3}He(K^-, Λp)n reaction at J-PARC is qualitatively well reproduced by the assumption that a $\bar{K}NN$ bound state is generated in the reaction, definitely discarding the interpretation in terms of an uncorrelated $\Lambda(1405)p$ state.

Subject Index D32

1. Introduction

The study of the $\bar{K}N$ interaction with coupled channels has been a traditional test field for chiral dynamics in its unitarized version. Since the pioneer works of Refs. [1,2], many works have been done in this field including also the contribution of the higher-order chiral Lagrangians (see recent review in Ref. [3]). One of the unexpected results was the finding of two poles for the $\Lambda(1405)$ resonance [4,5], which recently became official in the Particle Data Group [6] (see note on the $\Lambda(1405)$ [7]). The other issue that became topical was the possibility of having kaonic nuclei, in particular a bound $\bar{K}NN$ system. The study of this system has been thoroughly addressed theoretically [8–19] (see review paper in Ref. [20]), obtaining a binding energy that varies from a few MeV to 100 MeV. There are also discrepancies in the width of the state, which varies from 10 to 90 MeV. One step forward in the evaluation of the width was given in Ref. [21], where two-nucleon $\bar{K}$ absorption was explicitly considered. In that study a binding of 15–30 MeV was found, together with a width of the order of 80 MeV. The fact that the width is larger than the binding energy is shared by most of the theoretical approaches. One interesting point of view was to consider this system as a bound state of $\Lambda(1405)N$ [22]. This allows one to make some qualitative pictures that help to understand some of the results

Funded by SCOAP[3]

obtained when studying the possible formation of this system in different reactions. There have been previous claims of the formation of this state in some experiments, but soon the experimental signals were interpreted in terms of unavoidable conventional mechanisms (see overview in Refs. [20,23]). Yet, the experimental search has continued [24–28] with often contradictory views (see overview in Ref. [29]).

In this line, very recently, a peak structure was observed near the K^-pp threshold in the Λp invariant mass spectrum of the in-flight ^{3}He$(K^-, \Lambda p)n$ reaction of the J-PARC E15 experiment [29]. According to their analysis, this peak can be described by the Breit–Wigner formula with mass $M_X = 2355\,^{+6}_{-4}$(stat.) $\pm$ 12(sys.) MeV and width $\Gamma_X = 110\,^{+19}_{-17}$(stat.) $\pm$ 27(sys.)MeV. This structure could be a signal of the $\bar{K}NN(I = 1/2)$ bound state with a binding of $\sim$ 15 MeV from the K^-pp threshold.

In this paper we theoretically investigate the origin of the peak structure observed in the J-PARC E15 experiment. For this purpose, we take into account two possible mechanisms for producing a peak in the mass spectrum of the ^{3}He$(K^-, \Lambda p)n$ reaction. One corresponds to assuming the formation of a $\Lambda(1405)$ resonance that does not form a bound state with the remaining proton, while the other considers the formation of a bound state of the $\bar{K}NN$ system. We evaluate the cross section of the ^{3}He$(K^-, \Lambda p)n$ reaction assuming the $\bar{K}N \to \bar{K}N$ scattering around threshold and the $\Lambda(1405)$ resonance to be described by the chiral unitary approach [1,2,4,5], while the description of the $\bar{K}NN$ bound state is done in terms of the so-called fixed center approximation to the Faddeev equation [17,21].

As a result, we can unambiguously interpret the experimental spectrum in the scenario of a $\bar{K}NN$ broad bound state, obtained from the interaction of the $\bar{K}$ with a pair of nucleons [21]. In addition, in this scenario, we obtain a two peak structure of the mass spectrum near the $\bar{K}NN$ threshold. The peak below the threshold is the signal of the $\bar{K}NN$ bound state, while the peak above the threshold originates from the quasi-elastic scattering of the kaon in the first collision emitting a fast nucleon, in processes of the type $K^-n \to K^-n_{\rm escape}$ or $K^-p \to \bar{K}^0 n_{\rm escape}$.

This paper is organized as follows. In Sect. 2 we develop our formulation to obtain the cross section of the ^{3}He$(K^-, \Lambda p)n$ reaction, describing the details that allow us to obtain the scattering amplitude for the uncorrelated $\Lambda(1405)p$ mechanism and for the $\bar{K}NN$ bound state one. Next, in Sect. 3 we show our results and discuss the origin of the peak structure observed in the in-flight ^{3}He$(K^-, \Lambda p)n$ reaction in the J-PARC experiment. Section 4 is devoted to the conclusions of this study.

2. Formulation

In this section we formulate the cross section and scattering amplitude of the in-flight ^{3}He$(K^-, \Lambda p)n$ reaction. After showing the expression of the cross section in Sect. 2.1, we construct the scattering amplitude of the reaction in Sects. 2.2 and 2.3. In Sect. 2.2 we consider the case of an uncorrelated $\Lambda(1405)p$ system, i.e., the $\Lambda(1405)p$ system is generated without binding after emission of a fast neutron, and in Sect. 2.3 we take into account the multiple scattering of $\bar{K}$ between two nucleons to generate a $\bar{K}NN$ quasi-bound state.

According to the experimental condition, we concentrate on the three-nucleon absorption of K^-, i.e., we do not allow a spectator nucleon. Throughout this study, we take the global center-of-mass frame when we calculate the phase space for the cross section, while we evaluate the scattering amplitude in the ^{3}He rest frame so as to omit the center-of-mass momentum of ^{3}He in the wave function. Throughout this work the physical masses for the hadrons are used, except in the evaluation of the ^{3}He wave function and in the kaon propagators of the multiple scattering $\bar{K}NN$ amplitude.

2.1. *Cross section of the $^3He(K^-, \Lambda p)n$ reaction*

First we formulate the cross section for the $K^-(k)^3\mathrm{He}(P) \to \Lambda(p'_\Lambda)p(p'_p)n(p'_n)$ reaction, where the momenta of these particles are shown in parentheses. Since we are interested in the Λp spectrum as a function of its invariant mass $M_{\Lambda p}$, we fix the final-state phase space with the invariant mass $M_{\Lambda p}$, the solid angle for the neutron momentum in the global center-of-mass frame Ω_n, and the solid angle for Λ in the Λ-p rest frame Ω^*_Λ. With these quantities, the differential cross section can be expressed as [6]

$$\frac{d^2\sigma}{dM_{\Lambda p}d\cos\theta_n^{\mathrm{cm}}} = \frac{M_{^3\mathrm{He}}m_\Lambda m_p m_n}{(2\pi)^4 2p_{\mathrm{cm}}E_{\mathrm{cm}}^2}p'_n p^*_\Lambda \int d\Omega^*_\Lambda \overline{\sum_\lambda}\sum_{\lambda'}|\mathcal{T}|^2, \tag{1}$$

where we have performed the integral with respect to the azimuthal angle for the neutron momentum, which is irrelevant to the present formulation. In the expression, θ_n^{cm} is the neutron scattering angle in the global center-of-mass frame, $M_{^3\mathrm{He}}$, m_Λ, m_p, and m_n are the masses of ^{3}He, Λ, proton, and neutron, respectively, and p_{cm} and E_{cm} are the center-of-mass momentum and energy for the initial state:

$$p_{\mathrm{cm}} \equiv \frac{\lambda^{1/2}(E_{\mathrm{cm}}^2, m_{K^-}^2, M_{^3\mathrm{He}}^2)}{2E_{\mathrm{cm}}}, \quad E_{\mathrm{cm}} \equiv \left((k+P)^2\right)^{1/2} = \left(m_{K^-}^2 + M_{^3\mathrm{He}}^2 + 2\omega_{K^-}(\boldsymbol{k})M_{^3\mathrm{He}}\right)^{1/2}, \tag{2}$$

with the K^- mass m_{K^-}, the Källen function $\lambda(x,y,z) = x^2+y^2+z^2-2xy-2yz-2zx$, the initial kaon momentum in the laboratory frame k^μ, and $\omega_{K^-}(\boldsymbol{k}) \equiv \left(\boldsymbol{k}^2 + m_{K^-}^2\right)^{1/2}$. The momenta p'_n and p^*_Λ correspond to that of the neutron in the global center-of-mass frame and that of the Λ in the Λ-p rest frame, respectively, evaluated as

$$p'_n \equiv \frac{\lambda^{1/2}(E_{\mathrm{cm}}^2, M_{\Lambda p}^2, m_n^2)}{2E_{\mathrm{cm}}}, \quad p^*_\Lambda \equiv \frac{\lambda^{1/2}(M_{\Lambda p}^2, m_\Lambda^2, m_p^2)}{2M_{\Lambda p}}. \tag{3}$$

By means of the summation symbols in Eq. (1), we perform the average and sum of the squared scattering amplitude, $|\mathcal{T}|^2$, for the polarizations of the initial- and final-state particles, respectively.

From the double differential cross section $d^2\sigma/dM_{\Lambda p}d\cos\theta_n^{\mathrm{cm}}$, we can evaluate the mass spectrum $d\sigma/dM_{\Lambda p}$ and the differential cross section with respect to the neutron angle $d\sigma/d\cos\theta_n^{\mathrm{cm}}$ by performing the integral with respect to $\cos\theta_n^{\mathrm{cm}}$ and $M_{\Lambda p}$, respectively:

$$\frac{d\sigma}{dM_{\Lambda p}} = \int_{-1}^{1} d\cos\theta_n^{\mathrm{cm}} \frac{d^2\sigma}{dM_{\Lambda p}\,d\cos\theta_n^{\mathrm{cm}}}, \quad \frac{d\sigma}{d\cos\theta_n^{\mathrm{cm}}} = \int_{M_{\mathrm{min}}}^{M_{\mathrm{max}}} dM_{\Lambda p} \frac{d^2\sigma}{dM_{\Lambda p}\,d\cos\theta_n^{\mathrm{cm}}}, \tag{4}$$

where M_{min} and M_{max} are the lower and upper bounds of the invariant mass $M_{\Lambda p}$, respectively, which become $M_{\mathrm{min}} \sim 2.1$ GeV and $M_{\mathrm{max}} \sim 2.9$ GeV for an initial kaon momentum in the laboratory frame of $k_{\mathrm{lab}} = 1\,\mathrm{GeV}/c$, as that employed in the J-PARC E15 experiment [29]. In this study, however, we restrict those values to $M_{\mathrm{min}} = 2.2$ GeV and $M_{\mathrm{max}} = 2.6$ GeV, since we are interested only in the physics leading to a peak around the $\bar{K}NN$ threshold and we are ignoring other contributions that play only a background role in this region. We can also evaluate the total cross section as

$$\sigma = \int_{M_{\mathrm{min}}}^{M_{\mathrm{max}}} dM_{\Lambda p} \int_{-1}^{1} d\cos\theta_n^{\mathrm{cm}} \frac{d^2\sigma}{dM_{\Lambda p}\,d\cos\theta_n^{\mathrm{cm}}}. \tag{5}$$

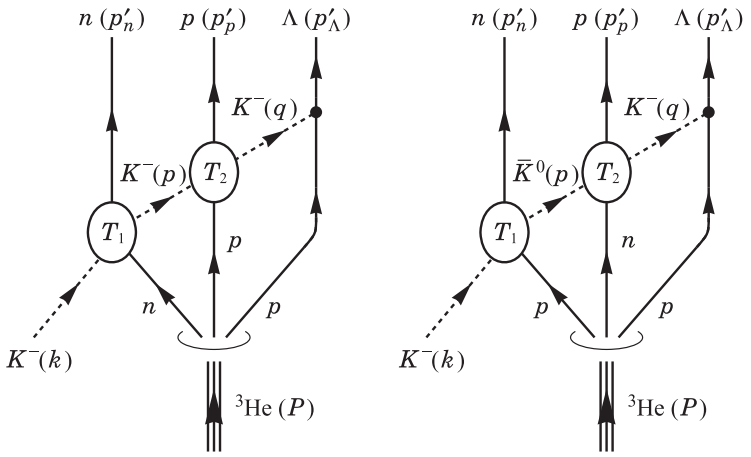

Fig. 1. Two Feynman diagrams most relevant to the three-nucleon absorption of K^- via an uncorrelated $\Lambda(1405)p$ system. We also show momenta of particles in parentheses.

2.2. *Scattering amplitude: Generating an uncorrelated* $\Lambda(1405)p$ *system*

Next we construct the scattering amplitude of the ^{3}He$(K^-, \Lambda p)n$ reaction with three-nucleon absorption of K^-. In this subsection we consider a case that an uncorrelated $\Lambda(1405)p$ system, without binding, is generated after the emission of a fast neutron. This process has a possibility of making a peak structure around the K^-pp threshold in the Λp invariant mass spectrum, since the $\Lambda(1405)$ resonance appears below the K^-p threshold. In Fig. 1 we show the two diagrams that implicitly contain the $\Lambda(1405)$ resonance in the intermediate state. In these diagrams, a fast neutron is emitted after the first collision of the K^- with a nucleon (T_1). Then, the second collision of the K^-p or the $\bar{K}^0 n$ (T_2) is enhanced at the energy of the $\Lambda(1405)$ resonance, producing an enhancement around the K^-pp threshold. Finally, the rescattered K^- is absorbed into a proton to become a Λ particle. An important point is that one expects a kaon, rather than another meson like the η or the pion, to be absorbed by the last nucleon because (1) the propagating kaon after the first collision is almost on its mass shell, hence the amplitude T_2 covers the region of the $\Lambda(1405)$ resonance, (2) the $\Lambda(1405)$ is expected to be a $\bar{K}N(I = 0)$ bound state [30–32], hence the process is dominated by the isospin $I = 0$ component of the $\bar{K}N$ interaction, and (3) the coupling strength of the $K^-p\Lambda$ vertex is strong while that of ηpp is very weak in flavor SU(3) symmetry [33,34].[1] Therefore, the most relevant diagrams for the reaction are the two shown in Fig. 1. The contribution from the uncorrelated $\Lambda(1405)p$ system will be observed as a peak in the Λp invariant mass spectrum.

Due to the antisymmetrization for the two protons in ^{3}He, we have two contributions from each diagram in Fig. 1. Therefore, the scattering amplitude of the reaction $\mathcal{T}$ can be expressed as

$$\mathcal{T} = \mathcal{T}_1 + \mathcal{T}_2 + \mathcal{T}_3 + \mathcal{T}_4. \tag{6}$$

The antisymmetrized ^{3}He wave function is given in Appendix A, and $\mathcal{T}_{1,2,3,4}$ come from the first, second, third, and fourth terms, respectively, of the ^{3}He wave function in Eq. (A.18).[2] In the following we give the explicit form of each amplitude $\mathcal{T}_i$.

[1] This latter vertex would appear in a mechanism where T_2 accounts for the $\bar{K}N \to \eta\Lambda$ scattering, followed by the ηNN Yukawa vertex.

[2] The last two terms in Eq. (A.18) have the neutron in the third place and induce a $\bar{K}^0 p \to \bar{K}^0 p$ interaction in T_2, which has $I = 1$ and hence is negligible compared to the $\Lambda(1405)$ excitation in $I = 0$.

Let us first fix the amplitude $\mathcal{T}_1$, which comes from the left diagram in Fig. 1. The momenta of the three nucleons in ^{3}He are denoted $p_1^\mu, p_2^\mu, p_3^\mu$ from left to right. Thus, we have

$$p_1^\mu = (p + p_n' - k)^\mu, \quad p_2^\mu = (q + p_p' - p)^\mu, \quad p_3^\mu = (p_\Lambda' - q)^\mu. \tag{7}$$

From these momenta, we can construct the momenta in Jacobi coordinates as in Appendix A, and here we show only the expressions relevant to the present formulation:

$$\begin{aligned} &\boldsymbol{P} = \boldsymbol{p}_1 + \boldsymbol{p}_2 + \boldsymbol{p}_3, \\ &\boldsymbol{p}_\lambda = \frac{2\boldsymbol{p}_1 - \boldsymbol{p}_2 - \boldsymbol{p}_3}{3} = \boldsymbol{p} + \boldsymbol{p}_n' - \boldsymbol{k} - \frac{1}{3}\boldsymbol{P}, \quad \boldsymbol{p}_\rho = \frac{\boldsymbol{p}_3 - \boldsymbol{p}_2}{2} = \frac{\boldsymbol{p} - 2\boldsymbol{q} + \boldsymbol{p}_\Lambda' - \boldsymbol{p}_p'}{2}. \end{aligned} \tag{8}$$

Then, by using a scheme similar to that developed in Refs. [35–38] and the ^{3}He wave function summarized in Appendix A, we can evaluate the scattering amplitude $\mathcal{T}_1$ as

$$\begin{aligned} -i\mathcal{T}_1 = &\int \frac{d^3q}{(2\pi)^3} \frac{i}{(q^0)^2 - \omega_{K^-}(\boldsymbol{q})^2} \int \frac{d^3p}{(2\pi)^3} \frac{i}{(p^0)^2 - \omega_{K^-}(\boldsymbol{p})^2 + im_{K^-}\Gamma_K} \tilde{\Psi}(p_\lambda, p_\rho) \\ &\times \left[-i\chi_p^\dagger T_2^{(K^-p \to K^-p)}(w_2)\chi_\uparrow \right] \left[-i\chi_n^\dagger T_1^{(K^-n \to K^-n)}(w_1, \cos\theta_1)\chi \right] \\ &\times \left[\tilde{V}\mathcal{F}(\boldsymbol{q})\boldsymbol{q} \left(\chi_\Lambda^\dagger \boldsymbol{\sigma} \chi_\downarrow \right) \right], \end{aligned} \tag{9}$$

where Γ_K is the kaon absorption width by two nucleons in the $\bar{K}NN$ system, whose value is fixed to be $\Gamma_K = 15$ MeV so as to reproduce the kaon absorption width of the $\bar{K}NN$ bound state in the fixed center approximation [21] (see Fig. 4 and related discussions below). We note that the exchanged kaon after the secondary scattering (q^μ) goes highly off its mass shell in the present kinematics, so the term $im_{K^-}\Gamma_K$ is unnecessary in the denominator of the corresponding propagator. The energies of the intermediate kaons are fixed in two ways: one employs the Watson approach [39] and the other one relies on the truncated Faddeev approach [40], which we refer to as options A and B, respectively. Namely, in option A we have [38]

$$q^0 = p_\Lambda'^0 - \left(m_p - \frac{B_{^3\mathrm{He}}}{3} \right), \tag{10}$$

$$p^0 = q^0 + p_p'^0 - \left(m_p - \frac{B_{^3\mathrm{He}}}{3} \right) = p_\Lambda'^0 + p_p'^0 - 2\left(m_p - \frac{B_{^3\mathrm{He}}}{3} \right), \tag{11}$$

with $B_{^3\mathrm{He}} = 7.7$ MeV being the ^{3}He binding energy, while in option B we have [40]

$$q^0 = p_\Lambda'^0 - \mathcal{E}_p(\boldsymbol{p}_\Lambda' - \boldsymbol{q}), \tag{12}$$

$$p^0 = q^0 + p_p'^0 - \mathcal{E}_p(\boldsymbol{q} + \boldsymbol{p}_p' - \boldsymbol{p}) = p_\Lambda'^0 + p_p'^0 - \mathcal{E}_p(\boldsymbol{p}_\Lambda' - \boldsymbol{q}) - \mathcal{E}_p(\boldsymbol{q} + \boldsymbol{p}_p' - \boldsymbol{p}), \tag{13}$$

where $\mathcal{E}_p(\boldsymbol{q}) \equiv m_p + \boldsymbol{q}^2/(2m_p)$. The Watson approach contains more contributions from diagrams of the rescattering of nucleons via the NN interaction, while the truncated Faddeev approach can give correct threshold behavior (see Ref. [38] for details).

The spinors χ, χ_Λ, χ_p, and χ_n stand for initial-state ^{3}He, and final-state Λ, proton, and neutron, respectively, all of which are either $\chi_\uparrow = (1,0)^t$ or $\chi_\downarrow = (0,1)^t$. Since we assume that the spin direction of ^{3}He equals that of the bound neutron, we take the same spinor for both of them. The ^{3}He

wave function $\tilde{\Psi}$ is evaluated with the harmonic oscillator potential, and its explicit form is given in Appendix A.[3]

The Yukawa $K^- p\Lambda$ vertex gives rise to Pauli matrices $\boldsymbol{\sigma}$ and a coupling constant $\tilde{V}$,

$$\tilde{V} = \alpha\frac{D+F}{2f} + \beta\frac{D-F}{2f}, \quad \alpha = \frac{2}{\sqrt{3}}, \quad \beta = -\frac{1}{\sqrt{3}}, \tag{14}$$

where f is the meson decay constant, taken to be $f = 93\,\mathrm{MeV}$, while $D = 0.795$ and $F = 0.465$ are adjusted to the weak decay of baryons. We also introduce a form factor

$$\mathcal{F}(\boldsymbol{q}) = \frac{\Lambda^2}{\Lambda^2 + \boldsymbol{q}^2} \tag{15}$$

for this vertex. We take a typical cutoff value $\Lambda = 0.8\,\mathrm{GeV}$, but the cutoff dependence of the cross section will be discussed later on.

The $K^- n \to K^- n$ scattering amplitude, $T_1^{(K^- n \to K^- n)}$, is a function of the center-of-mass energy for the initial kaon-bound neutron system, w_1, and the scattering angle in their center-of-mass frame θ_1, both of which are evaluated by neglecting the Fermi motion of the bound neutron. As a result, we have

$$w_1 = \left((k+p_1)^2\right)^{1/2} \approx \left(\left(k^0 + m_n - B_{^3\mathrm{He}}/3\right)^2 - \boldsymbol{k}^2\right)^{1/2}, \tag{16}$$

$$\cos\theta_1 = \frac{m_n^2 + m_{K^-}^2 - 2\omega_{K^-}(p_{K^-}(w_1))E_n(w_1) - (p_n' - k)^2}{2p_{K^-}(w_1)^2}, \tag{17}$$

where

$$p_{K^-}(w_1) \equiv \frac{\lambda^{1/2}(w_1^2, m_{K^-}^2, m_n^2)}{2w_1}, \quad E_n(w_1) \equiv \frac{w_1^2 + m_n^2 - m_{K^-}^2}{2w_1}. \tag{18}$$

We note that the value of the right-hand side in Eq. (17) may become larger than 1 or smaller than -1 because the bound nucleons actually have an energy and momentum distribution different to the free one. In such a case we take $\cos\theta_1 = 1$ or -1, respectively. Now that w_1 and θ_1 are fixed by the momenta of the initial- and final-state particles, we can put $T_1^{(K^- n \to K^- n)}$ outside of the integral. In addition, for this amplitude T_1 we neglect the spin flip contribution, and hence we can factorize the spinor part $\chi_n^\dagger \chi$. The amplitude $T_1^{(K^- n \to K^- n)}$ is evaluated phenomenologically in Appendix B.

The $K^- p \to K^- p$ scattering amplitude $T_2^{(K^- p \to K^- p)}$ is a function of the center-of-mass energy for the exchanged kaon (q^μ) and final-state proton, w_2:

$$w_2 = \left((q + p_p')^2\right)^{1/2} = \left((q^0 + p_p'^0)^2 - |\boldsymbol{q} + \boldsymbol{p}_p'|^2\right)^{1/2}. \tag{19}$$

Since the energies relevant to our study are those near the $K^- p$ threshold, we consider only the s-wave part of the amplitude $T_2^{(K^- p \to K^- p)}$. We calculate this $K^- p \to K^- p$ amplitude in the so-called chiral

[3] We would have a factor $1/\sqrt{6}$ from the ^{3}He wave function as in Eq. (A.18), but this factor will be compensated in the cross section by the identical contributions of six diagrams of different topology. These correspond to having the first scattering, T_1, in either of the three nucleons and the second scattering, T_2, in either of the remaining two nucleons. The final states have the triplet $np\Lambda$ produced in different order and these contributions add incoherently in the cross section.

unitary approach [1,2,4,5], where the $\Lambda(1405)$ resonance is dynamically generated from the meson–baryon degrees of freedom. For the chiral unitary amplitude we take into account ten channels: K^-p, $\bar{K}^0n$, $\pi^0\Lambda$, $\pi^0\Sigma^0$, $\pi^+\Sigma^-$, $\pi^-\Sigma^+$, $\eta\Lambda$, $\eta\Sigma^0$, $K^0\Xi^0$, and $K^+\Xi^-$. The formulation of the amplitude T_2 in the chiral unitary approach is summarized in Appendix C. An important point is that in this amplitude we take into account the kaon absorption by two nucleons in the $\bar{K}NN$ system effectively via the inclusion of a width Γ_K in the kaon propagator [see Fig. C.1(a) in Appendix C].

As a consequence, the explicit form of $\mathcal{T}_1$ finally becomes

$$\begin{aligned}\mathcal{T}_1 =& i\left(\chi_n^\dagger \chi\right)\left(\chi_p^\dagger \chi_\uparrow\right) \times T_1^{(K^-n\to K^-n)}(w_1,\cos\theta_1)\tilde{V}\int \frac{d^3q}{(2\pi)^3}\frac{\mathcal{F}(\boldsymbol{q})\boldsymbol{q}\left(\chi_\Lambda^\dagger \boldsymbol{\sigma}\chi_\downarrow\right)}{(q^0)^2-\omega_{K^-}(\boldsymbol{q})^2}\\ &\times T_2^{(K^-p\to K^-p)}(w_2)\int \frac{d^3p}{(2\pi)^3}\frac{1}{(p^0)^2-\omega_{K^-}(\boldsymbol{p})^2+im_{K^-}\Gamma_K}\tilde{\Psi}(p_\lambda,p_\rho).\end{aligned} \tag{20}$$

In a similar manner, we can write the formulas of the other scattering amplitudes. Here we note that, although one needs to antisymmetrize the momentum and spin of the nucleons in ^{3}He, the wave function $\tilde{\Psi}(p_\lambda,p_\rho)$ in Eq. (A.15) is unchanged for the exchange of momenta $\boldsymbol{p}_i \leftrightarrow \boldsymbol{p}_j$ (i, $j = 1$, 2, and 3), since the global argument of the Gaussian functions in $\tilde{\Psi}(p_\lambda,p_\rho)$ reduces to $\left(\boldsymbol{P}^2/3-\sum_{i=1}^3\boldsymbol{p}_i^2\right)/(2m_N\omega_\lambda)$. Therefore, we have to consider the antisymmetrization of the spin variables only, and we have

$$\begin{aligned}\mathcal{T}_2 =& -i\left(\chi_n^\dagger \chi\right)\left(\chi_p^\dagger \chi_\downarrow\right) T_1^{(K^-n\to K^-n)}(w_1,\cos\theta_1)\tilde{V}\int \frac{d^3q}{(2\pi)^3}\frac{\mathcal{F}(\boldsymbol{q})\boldsymbol{q}\left(\chi_\Lambda^\dagger \boldsymbol{\sigma}\chi_\uparrow\right)}{(q^0)^2-\omega_{K^-}(\boldsymbol{q})^2}\\ &\times T_2^{(K^-p\to K^-p)}(w_2)\int \frac{d^3p}{(2\pi)^3}\frac{1}{(p^0)^2-\omega_{K^-}(\boldsymbol{p})^2+im_{K^-}\Gamma_K}\tilde{\Psi}(p_\lambda,p_\rho),\end{aligned} \tag{21}$$

$$\begin{aligned}\mathcal{T}_3 =& -i\left(\chi_n^\dagger \chi_\uparrow\right)\left(\chi_p^\dagger \chi\right) T_1^{(K^-p\to \bar{K}^0n)}(w_1',\cos\theta_1')\tilde{V}\int \frac{d^3q}{(2\pi)^3}\frac{\mathcal{F}(\boldsymbol{q})\boldsymbol{q}\left(\chi_\Lambda^\dagger \boldsymbol{\sigma}\chi_\downarrow\right)}{(q^0)^2-\omega_{K^-}(\boldsymbol{q})^2}\\ &\times T_2^{(\bar{K}^0n\to K^-p)}(w_2)\int \frac{d^3p}{(2\pi)^3}\frac{1}{(p'^0)^2-\omega_{\bar{K}^0}(\boldsymbol{p})^2+im_{\bar{K}^0}\Gamma_K}\tilde{\Psi}(p_\lambda,p_\rho),\end{aligned} \tag{22}$$

$$\begin{aligned}\mathcal{T}_4 =& i\left(\chi_n^\dagger \chi_\downarrow\right)\left(\chi_p^\dagger \chi\right) T_1^{(K^-p\to \bar{K}^0n)}(w_1',\cos\theta_1')\tilde{V}\int \frac{d^3q}{(2\pi)^3}\frac{\mathcal{F}(\boldsymbol{q})\boldsymbol{q}\left(\chi_\Lambda^\dagger \boldsymbol{\sigma}\chi_\uparrow\right)}{(q^0)^2-\omega_{K^-}(\boldsymbol{q})^2}\\ &\times T_2^{(\bar{K}^0n\to K^-p)}(w_2)\int \frac{d^3p}{(2\pi)^3}\frac{1}{(p'^0)^2-\omega_{\bar{K}^0}(\boldsymbol{p})^2+im_{\bar{K}^0}\Gamma_K}\tilde{\Psi}(p_\lambda,p_\rho).\end{aligned} \tag{23}$$

Here $\omega_{\bar{K}^0}(\boldsymbol{p}) \equiv \left(\boldsymbol{p}^2+m_{\bar{K}^0}^2\right)^{1/2}$ with the $\bar{K}^0$ mass $m_{\bar{K}^0}$ and w_1' and $\cos\theta_1'$ are fixed in the same manner as in Eqs. (16) and (17), respectively, but for the $K^-p\to\bar{K}^0n$ reaction instead of the $K^-n\to K^-n$ one. The energy p'^0 is fixed as

$$p'^0 = \begin{cases} p_\Lambda'^0 + p_p'^0 - \left(m_p+m_n-\dfrac{2}{3}B_{^3\mathrm{He}}\right) & \text{in option A,}\\ p_\Lambda'^0 + p_p'^0 - \mathcal{E}_p(\boldsymbol{p}_\Lambda'-\boldsymbol{q}) - \mathcal{E}_n(\boldsymbol{q}+\boldsymbol{p}_p'-\boldsymbol{p}) & \text{in option B,}\end{cases} \tag{24}$$

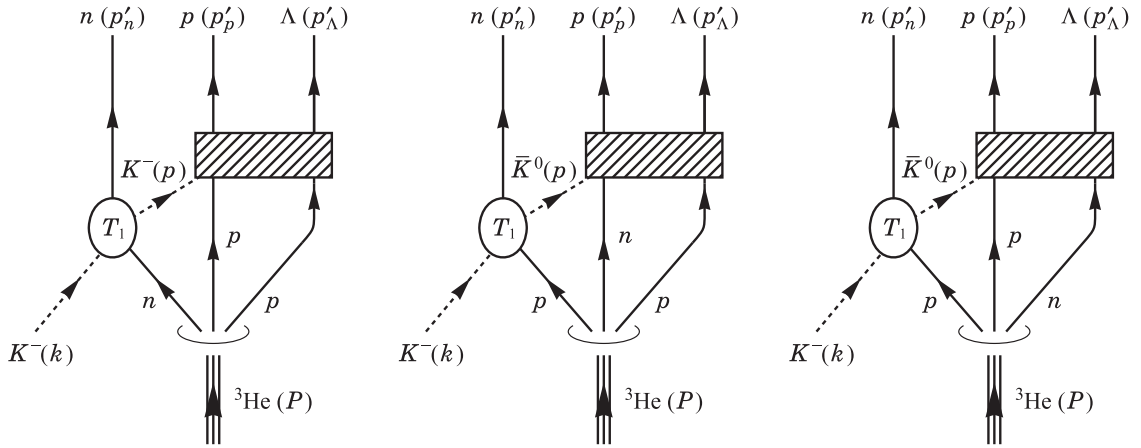

Fig. 2. The three most relevant Feynman diagrams depicting the three-nucleon absorption of a K^- implementing the multiple kaon scattering between two nucleons, which is represented by the shaded rectangles (see Fig. 3).

with $\mathcal{E}_n(\boldsymbol{q}) \equiv m_n + \boldsymbol{q}^2/(2m_n)$, where p'^0 is different from p^0 as the former contains the neutron mass or energy. The amplitudes $T_1^{(K^-n\to K^-n)}$ and $T_1^{(K^-p\to \bar{K}^0n)}$ are evaluated phenomenologically in Appendix B, while the amplitudes $T_2^{(K^-p\to K^-p)}$ and $T_2^{(\bar{K}^0n\to K^-p)}$ are taken from a chiral unitary approach in s wave, as described in Appendix C.

2.3. *Scattering amplitude: Generating a $\bar{K}NN$ quasi-bound state*

In this subsection we consider the case of the formation of a $\bar{K}NN$ quasi-bound state in the $^3\mathrm{He}(K^-, \Lambda p)n$ reaction, which would be the origin of the peak structure seen in the J-PARC E15 experiment. The $\bar{K}NN$ quasi-bound state is generated as the multiple scattering of the kaon between two nucleons after emission of a fast neutron in the reaction. The most relevant diagrams are shown in Fig. 2.

Taking into account the antisymmetrization for three nucleons, we have six contributions to the scattering amplitude of the reaction:

$$\mathcal{T} = \mathcal{T}_1 + \mathcal{T}_2 + \mathcal{T}_3 + \mathcal{T}_4 + \mathcal{T}_5 + \mathcal{T}_6. \tag{25}$$

The amplitudes $\mathcal{T}_{1,2,3,4,5,6}$ come from the first, second, third, fourth, fifth, and sixth terms, respectively, of the ^{3}He wave function in Eq. (A.18) in Appendix A.

Let us consider the first term $\mathcal{T}_1$. We can use the same form as in Eq. (20), keeping the scattering amplitude of the first step, $T_1^{(K^-n\to K^-n)}$, the K^- propagator of p^μ, and the ^{3}He wave function. Then, the most important part of the scattering amplitude, i.e., the part where the $\bar{K}NN$ quasi-bound state is generated and the kaon is absorbed, remains to be implemented. This is represented by the diagrams shown in Fig. 3, which are calculated as follows. First, we do not consider spin flips during the multiple scattering since the process takes place near the $\bar{K}NN$ threshold. Therefore, the spinor factor $\left(\chi_p^\dagger \chi_\uparrow\right)\left(\chi_\Lambda^\dagger \boldsymbol{\sigma}\chi_\downarrow\right)$ is the same as in Eq. (20). Second, the multiple scattering amplitude of Fig. 3 is calculated employing the so-called fixed center approximation to the Faddeev equation [17,21], and we denote this part as T^{FCA}. Third, the kaon absorption takes place after the multiple scattering,

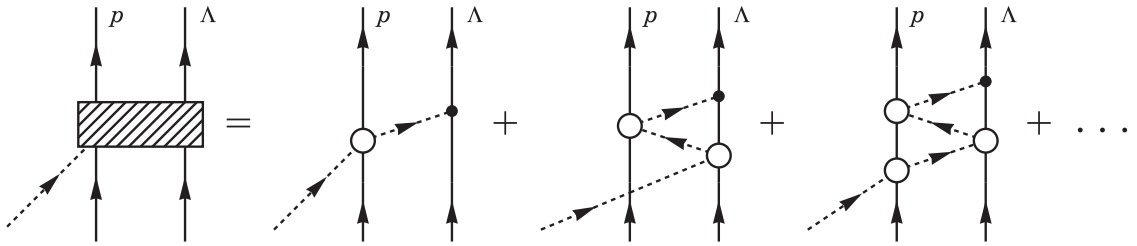

Fig. 3. Diagrammatic equation for the kaon absorption amplitudes after multiple scattering. They contain multiple scattering amplitudes, which are evaluated in the fixed center approximation. The unspecified dashed and solid lines are $\bar{K}$ and N, respectively. The open circles are the $\bar{K}N \to \bar{K}N$ scattering amplitude evaluated in the chiral unitary approach and the dots represent the $\bar{K}N\Lambda$ vertex.

which is to be evaluated in the same manner as the $K^- p\Lambda$ vertex in Eq. (20). Here, we have two types of vertices, $K^- p\Lambda$ and $\bar{K}^0 n\Lambda$, and both have the same structure and coupling constant as in Eq. (14). As a consequence, the scattering amplitude $\mathcal{T}_1$ can be obtained by replacing $T_2^{(K^- p \to K^- p)}$ with $T^{\rm FCA}$ in Eq. (20) as

$$\mathcal{T}_1 = i\left(\chi_n^\dagger \chi\right)\left(\chi_p^\dagger \chi_\uparrow\right) T_1^{(K^- n \to K^- n)}(w_1, \cos\theta_1)\tilde{V}\int \frac{d^3q}{(2\pi)^3}\mathcal{F}(\boldsymbol{q})\boldsymbol{q}\left(\chi_\Lambda^\dagger \boldsymbol{\sigma}\chi_\downarrow\right)$$
$$\times\left[\frac{T_{11}^{\rm FCA}+T_{41}^{\rm FCA}}{(q^0)^2-\omega_{K^-}(\boldsymbol{q})^2}+\frac{T_{13}^{\rm FCA}+T_{43}^{\rm FCA}}{(q^0)^2-\omega_{\bar{K}^0}(\boldsymbol{q})^2}\right]\int\frac{d^3p}{(2\pi)^3}\frac{\tilde{\Psi}(p_\lambda,p_\rho)}{(p^0)^2-\omega_{K^-}(\boldsymbol{p})^2+im_{K^-}\Gamma_K}, \quad (26)$$

where everything, except for the amplitude of the multiple scattering $T^{\rm FCA}$, is evaluated as in Eq. (20). In particular, the energies of the kaons, p^0 and q^0, are fixed by the option A or B.

The multiple scattering amplitude $T_{ij}^{\rm FCA}$ is labeled by channel indices i and j. Since we have the $\bar{K}NN$ system decaying into Λp, we consider six channels in the order $K^- pp$, $\bar{K}^0 np$, $\bar{K}^0 pn$, ppK^-, $np\bar{K}^0$, and $pn\bar{K}^0$. In this study, we neglect diagrams with pion exchange between two nucleons in the $T_{ij}^{\rm FCA}$ amplitude, since these contributions are found to be small (see Appendix D). We note that we distinguish the ordering of the kaon and the two nucleons; in channels where the kaon appears first (last), the kaon interacts with the first (second) nucleon of the ordering at the first or last of the scatterings. In this sense, the term $T_{11}^{\rm FCA}$ ($T_{41}^{\rm FCA}$) in Eq. (26) represents the multiple $K^- pp$ (ppK^-) $\to K^- pp$ scattering, which means that the K^- scatters with the nucleon on the left (right) in the entrance channel and with that on the left in the exit one. In other words, $T_{11}^{\rm FCA}$ and $T_{41}^{\rm FCA}$ come from odd- and even-numbered interaction diagrams in the right-hand side of Fig. 3. Then, the sum $T_{11}^{\rm FCA}+T_{41}^{\rm FCA}$ represents the whole of the multiple scattering amplitude in Fig. 3. For these terms, the K^- is absorbed via the $K^- p\Lambda$ vertex. Similarly, the terms $T_{13}^{\rm FCA}$ and $T_{43}^{\rm FCA}$ represent $K^- pp$ and $ppK^- \to \bar{K}^0 pn$ scatterings, respectively, and the $\bar{K}^0$ is absorbed via the $\bar{K}^0 n\Lambda$ vertex. Since we fix the ordering of the final state in the reaction as $np\Lambda$ from left to right, the final-state channel of the multiple scattering should be 1 or 3, where the kaon is absorbed by the second nucleon of the pair after the interaction with the first one which emits the proton. We also note that the multiple scattering amplitude in the fixed center approximation is a function of the invariant mass $M_{\Lambda p}$. The formulation of the fixed center approximation is given in Appendix D, and the details are given in Refs. [17,21].

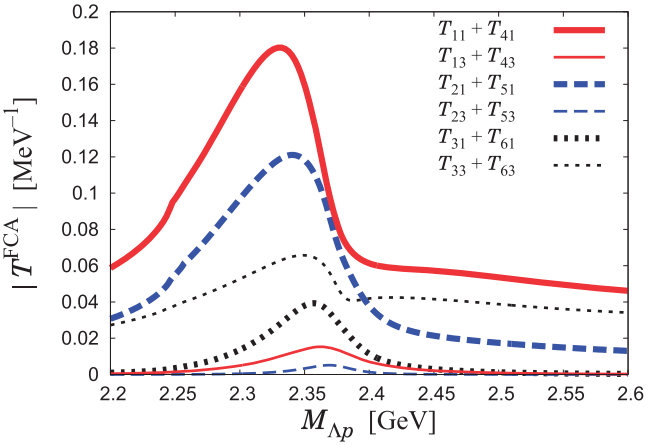

Fig. 4. Absolute values of the kaon multiple amplitudes evaluated in the fixed center approximation.

In a similar manner, we can calculate the amplitudes $\mathcal{T}_{2,3,4,5,6}$ as

$$\mathcal{T}_2 = -i\left(\chi_n^\dagger \chi\right)\left(\chi_p^\dagger \chi_\downarrow\right) T_1^{(K^- n\to K^- n)}(w_1,\cos\theta_1)\tilde{V}\int\frac{d^3q}{(2\pi)^3}\mathcal{F}(\boldsymbol{q})\boldsymbol{q}\left(\chi_\Lambda^\dagger \boldsymbol{\sigma}\chi_\uparrow\right)$$
$$\times\left[\frac{T_{11}^{\rm FCA}+T_{41}^{\rm FCA}}{(q^0)^2-\omega_{K^-}(\boldsymbol{q})^2}+\frac{T_{13}^{\rm FCA}+T_{43}^{\rm FCA}}{(q^0)^2-\omega_{\bar{K}^0}(\boldsymbol{q})^2}\right]\int\frac{d^3p}{(2\pi)^3}\frac{\tilde{\Psi}(p_\lambda,p_\rho)}{(p^0)^2-\omega_{K^-}(\boldsymbol{p})^2+im_{K^-}\Gamma_K}, \quad (27)$$

$$\mathcal{T}_3 = -i\left(\chi_n^\dagger \chi_\uparrow\right)\left(\chi_p^\dagger \chi\right) T_1^{(K^- p\to \bar{K}^0 n)}(w_1',\cos\theta_1')\tilde{V}\int\frac{d^3q}{(2\pi)^3}\mathcal{F}(\boldsymbol{q})\boldsymbol{q}\left(\chi_\Lambda^\dagger \boldsymbol{\sigma}\chi_\downarrow\right)$$
$$\times\left[\frac{T_{21}^{\rm FCA}+T_{51}^{\rm FCA}}{(q^0)^2-\omega_{K^-}(\boldsymbol{q})^2}+\frac{T_{23}^{\rm FCA}+T_{53}^{\rm FCA}}{(q^0)^2-\omega_{\bar{K}^0}(\boldsymbol{q})^2}\right]\int\frac{d^3p}{(2\pi)^3}\frac{\tilde{\Psi}(p_\lambda,p_\rho)}{(p'^0)^2-\omega_{\bar{K}^0}(\boldsymbol{p})^2+im_{\bar{K}^0}\Gamma_K}, \quad (28)$$

$$\mathcal{T}_4 = i\left(\chi_n^\dagger \chi_\downarrow\right)\left(\chi_p^\dagger \chi\right) T_1^{(K^- p\to \bar{K}^0 n)}(w_1',\cos\theta_1')\tilde{V}\int\frac{d^3q}{(2\pi)^3}\mathcal{F}(\boldsymbol{q})\boldsymbol{q}\left(\chi_\Lambda^\dagger \boldsymbol{\sigma}\chi_\uparrow\right)$$
$$\times\left[\frac{T_{21}^{\rm FCA}+T_{51}^{\rm FCA}}{(q^0)^2-\omega_{K^-}(\boldsymbol{q})^2}+\frac{T_{23}^{\rm FCA}+T_{53}^{\rm FCA}}{(q^0)^2-\omega_{\bar{K}^0}(\boldsymbol{q})^2}\right]\int\frac{d^3p}{(2\pi)^3}\frac{\tilde{\Psi}(p_\lambda,p_\rho)}{(p'^0)^2-\omega_{\bar{K}^0}(\boldsymbol{p})^2+im_{\bar{K}^0}\Gamma_K}, \quad (29)$$

$$\mathcal{T}_5 = i\left(\chi_n^\dagger \chi_\uparrow\right)\left(\chi_p^\dagger \chi_\downarrow\right) T_1^{(K^- p\to \bar{K}^0 n)}(w_1',\cos\theta_1')\tilde{V}\int\frac{d^3q}{(2\pi)^3}\mathcal{F}(\boldsymbol{q})\boldsymbol{q}\left(\chi_\Lambda^\dagger \boldsymbol{\sigma}\chi\right)$$
$$\times\left[\frac{T_{31}^{\rm FCA}+T_{61}^{\rm FCA}}{(q^0)^2-\omega_{K^-}(\boldsymbol{q})^2}+\frac{T_{33}^{\rm FCA}+T_{63}^{\rm FCA}}{(q^0)^2-\omega_{\bar{K}^0}(\boldsymbol{q})^2}\right]\int\frac{d^3p}{(2\pi)^3}\frac{\tilde{\Psi}(p_\lambda,p_\rho)}{(p'^0)^2-\omega_{\bar{K}^0}(\boldsymbol{p})^2+im_{\bar{K}^0}\Gamma_K}, \quad (30)$$

$$\mathcal{T}_6 = -i\left(\chi_n^\dagger \chi_\downarrow\right)\left(\chi_p^\dagger \chi_\uparrow\right) T_1^{(K^- p\to \bar{K}^0 n)}(w_1',\cos\theta_1')\tilde{V}\int\frac{d^3q}{(2\pi)^3}\mathcal{F}(\boldsymbol{q})\boldsymbol{q}\left(\chi_\Lambda^\dagger \boldsymbol{\sigma}\chi\right)$$
$$\times\left[\frac{T_{31}^{\rm FCA}+T_{61}^{\rm FCA}}{(q^0)^2-\omega_{K^-}(\boldsymbol{q})^2}+\frac{T_{33}^{\rm FCA}+T_{63}^{\rm FCA}}{(q^0)^2-\omega_{\bar{K}^0}(\boldsymbol{q})^2}\right]\int\frac{d^3p}{(2\pi)^3}\frac{\tilde{\Psi}(p_\lambda,p_\rho)}{(p'^0)^2-\omega_{\bar{K}^0}(\boldsymbol{p})^2+im_{\bar{K}^0}\Gamma_K}. \quad (31)$$

In Fig. 4 we show the absolute values of the kaon multiple amplitudes $T_{11}^{\rm FCA}+T_{41}^{\rm FCA}$, $T_{13}^{\rm FCA}+T_{43}^{\rm FCA}$, $T_{21}^{\rm FCA}+T_{51}^{\rm FCA}$, $T_{23}^{\rm FCA}+T_{53}^{\rm FCA}$, $T_{31}^{\rm FCA}+T_{61}^{\rm FCA}$, and $T_{33}^{\rm FCA}+T_{63}^{\rm FCA}$, which are evaluated in the fixed center approximation as functions of $M_{\Lambda p}$. As one can see from the figure, the amplitudes $T^{\rm FCA}$ show a peak around $M_{\Lambda p}=2.35\,\text{GeV}$, which corresponds to a signal of the $\bar{K}NN$ quasi-bound state in

our approach. Therefore, in the Λp invariant mass spectrum of the ${}^3\mathrm{He}(K^-, \Lambda p)n$ reaction, we will observe such a peak structure if the strength of the peak for the signal of the $\bar{K}NN$ quasi-bound state is strong enough. The amplitude $|T_{11}^{\mathrm{FCA}} + T_{41}^{\mathrm{FCA}}|$ has the strongest signal peak, since the $\bar{K}NN$ quasi-bound state is generated dominantly by the $K^-p \to K^-p$ scattering in the K^-pp configuration. Here we note that the kaon absorption width Γ_K is fixed as 15 MeV, so that the amplitude $T_{11}^{\mathrm{FCA}} + T_{41}^{\mathrm{FCA}}$ reproduces the width of the $\bar{K}NN$ bound-state signal in Ref. [21]. We also note that we cannot see a clear $\bar{K}NN$ threshold around 2.37 GeV in the amplitude T^{FCA} in Fig. 4 because we introduce a finite width for the kaon propagators of the amplitude. In contrast, the cusp at 2.25 GeV is caused by the $\pi\Sigma N$ threshold, where the $\pi\Sigma$ degrees of freedom are intrinsically contained in the two-body chiral $\bar{K}N \to \bar{K}N$ amplitudes employed in the construction of the T^{FCA} amplitudes.

3. Numerical results

In this section we show the numerical results of our calculations for the cross section of the ${}^3\mathrm{He}(K^-, \Lambda p)n$ reaction. We fix the initial kaon momentum in the laboratory frame to be $k_{\mathrm{lab}} = 1\,\mathrm{GeV}/c$, as in the experiment [29]. We note that the momentum of the intermediate kaon after the first $K^-n \to K^-n_{\mathrm{escape}}$ or $K^-p \to \bar{K}^0 n_{\mathrm{escape}}$ collision becomes $\lesssim 50\,\mathrm{MeV}/c$ for an initial kaon momentum of $k_{\mathrm{lab}} = 1\,\mathrm{GeV}/c$, if the escaping neutron goes forward. This means that the initial K^- energy chosen favors the production of low energy kaons and is suitable for seeing a possible $\bar{K}NN$ state around its threshold.

As mentioned before, we consider two scenarios to reproduce a peak structure in the Λp invariant mass spectrum of the ${}^3\mathrm{He}(K^-, \Lambda p)n$ reaction. One consists of generating the $\Lambda(1405)$ but not allowing it to form a bound state with the remaining proton. The uncorrelated $\Lambda(1405)p$ system eventually decays into a Λp pair. The other consists of generating a $\bar{K}NN$ quasi-bound state that subsequently decays into Λp. The numerical results of the spectra in these two scenarios are shown in Sects. 3.1 and 3.2, respectively.

Our numerical results are compared with the experimental data [29] and in particular with their analysis in terms of a Breit–Wigner amplitude

$$\frac{d\sigma}{dM_{\Lambda p}} \propto p'_n p^*_\Lambda \frac{\Gamma_X^2}{(M_{\Lambda p} - M_X)^2 + \Gamma_X^2/4}, \tag{32}$$

with parameters $M_X = 2355\,^{+6}_{-4}(\mathrm{stat.}) \pm 12(\mathrm{sys.})\,\mathrm{MeV}$ and $\Gamma_X = 110\,^{+19}_{-17}(\mathrm{stat.}) \pm 27(\mathrm{sys.})\,\mathrm{MeV}$ [29].[4] The comparison between our results and this mass spectrum helps us to discuss the origin of the peak structure in the invariant mass spectrum.

3.1. *Generating an uncorrelated* $\Lambda(1405)p$ *system*

First, we consider the case that the uncorrelated $\Lambda(1405)p$ system is generated in the in-flight ${}^3\mathrm{He}(K^-, \Lambda p)n$ reaction, as formulated in Sect. 2.2. The numerical results of the differential cross section are shown in Figs. 5 and 6 for options A and B, respectively.

As seen from Figs. 5 and 6, in both options A and B, we find the peak of the invariant mass spectrum $d\sigma/dM_{\Lambda p}$ at around the K^-pp threshold, $M_{\Lambda p} \approx m_{K^-} + m_p + m_p = 2.370\,\mathrm{GeV}$. This corresponds to the signal of the uncorrelated $\Lambda(1405)p$. Here we emphasize that the uncorrelated $\Lambda(1405)p$ gives a peak not at the $\Lambda(1405)p$ threshold, which is about 2.355 GeV in our model, but just at the K^-pp

[4] We note that the parameters for this mass spectrum as well as the experimental data shown in the figures were obtained without acceptance corrections.

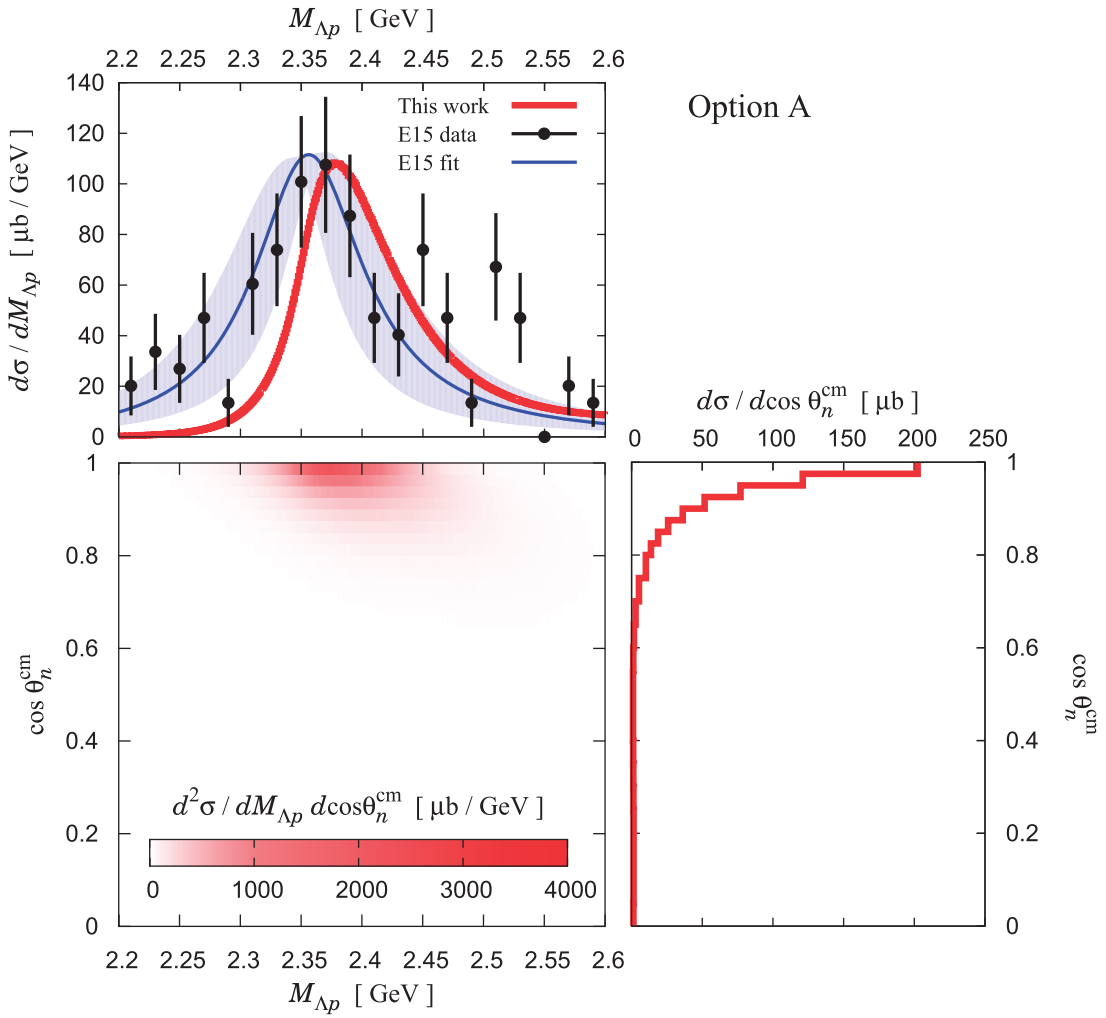

Fig. 5. Differential cross section of the in-flight ^{3}He$(K^-, \Lambda p)n$ reaction for the uncorrelated $\Lambda(1405)p$ system (see Fig. 1) with option A. The experimental (E15) data for the mass spectrum $d\sigma/dM_{\Lambda p}$ and its fit [Eq. (32)] are taken from Ref. [29] and are shown in arbitrary units.

threshold in option A or at 2.4 GeV in option B. This is because the $\Lambda(1405)$ is slowly moving due to the momentum $\boldsymbol{p}$ carried by the kaon after the first scattering, and hence the moving $\Lambda(1405)$ and the proton (the third nucleon of ^{3}He) have an invariant mass larger than the $\Lambda(1405)p$ threshold.

However, regardless of the option A or B, the peak position is not consistent with the experimental data and their fit [Eq. (32)], which are shown in Figs. 5 and 6 in arbitrary units. The peak position in the experiment is more than 20 MeV lower than that of our result in the uncorrelated $\Lambda(1405)p$ case. In addition, we cannot reproduce the behavior of the tail of the peak below the K^-pp threshold, say at $M_{\Lambda p} = 2.3$ GeV. This fact indicates that the experimental signal observed in the in-flight ^{3}He$(K^-, \Lambda p)n$ reaction at J-PARC [29] is definitely not the uncorrelated $\Lambda(1405)p$ state.

In Figs. 5 and 6, we also show the behavior of the angular distribution of the cross section $d\sigma/d\cos\theta_n^{\rm cm}$, as well as the double differential cross section $d^2\sigma/dM_{\Lambda p}d\cos\theta_n^{\rm cm}$. Here we show the results only in the region $\cos\theta_n^{\rm cm} \geq 0$, since there is no significant contribution in the region $\cos\theta_n^{\rm cm} < 0$. From the figure, one can see that the uncorrelated $\Lambda(1405)p$ signal comes dominantly from the condition of forward neutron emission, i.e., $\theta_n^{\rm cm} \approx 0$ degrees. This has both kinematic and dynamical causes. As far as kinematics is concerned, we note that for finite scattering angle

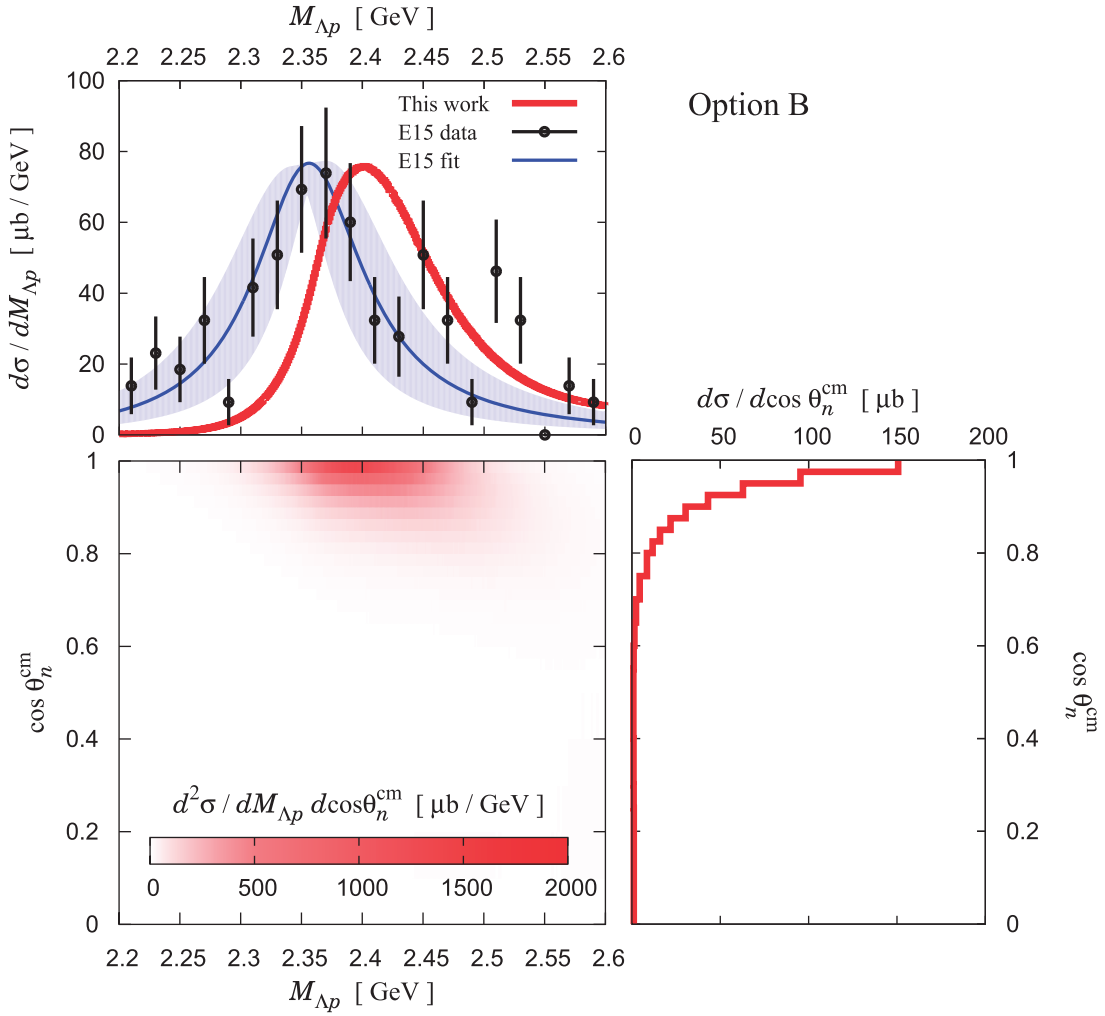

Fig. 6. The same as Fig. 5 for the kinematic option B.

$\theta_n^{\rm cm} > 0$ degrees, the kaon momenta in the intermediate states $|\boldsymbol{p}|$ and $|\boldsymbol{q}|$ become large and are comparable to the initial kaon momentum 1 GeV/c in the laboratory frame. Therefore, the kaon propagator $1/[(q^0)^2 - \boldsymbol{q}^2 - m_K^2]$ and the form factor $\mathcal{F}(\boldsymbol{q})$ suppress the cross section for $\theta_n^{\rm cm} > 0$ degrees.[5] With respect to the dynamics, we observe that the cross sections of $K^- p \to \bar{K}^0 n$ and $K^- n \to K^- n$ at $k_{\rm lab} = 1\,{\rm GeV}/c$ have a local maximum for forward neutron emission, as seen in Fig. B.1 in Appendix B, and hence the forward neutron emission is also favored in the $^3{\rm He}(K^-, \Lambda p)n$ reaction. For these reasons, the uncorrelated $\Lambda(1405)p$ signal favors the condition of forward neutron emission, $\theta_n^{\rm cm} \approx 0$ degrees.[6] We also note that the peak shifts slightly upwards as the scattering angle $\theta_n^{\rm cm}$ increases, which means that the $\Lambda(1405)$ gets more momentum from the kaon after the first scattering. This contribution can be seen as the band from the $\bar{K}NN$ threshold at $\cos\theta_n^{\rm cm} = 1$ to the lower-right direction in the $d^2\sigma/dM_{\Lambda p} d\cos\theta_n^{\rm cm}$ plot of the figures, although its strength is very weak due to the kinematic and dynamical reasons explained above.

[5] Since $(q^0)^2 - m_K^2$ is always negative in the present kinematics, the square of this propagator, $1/[(q^0)^2 - \boldsymbol{q}^2 - m_K^2]^2$, monotonically decreases as $|\boldsymbol{q}|$ increases.

[6] This means that the neutron goes in the opposite direction to the original one in the $K^- n \to K^- n$ center-of-mass frame, and equivalently the kaon goes backwards in that frame.

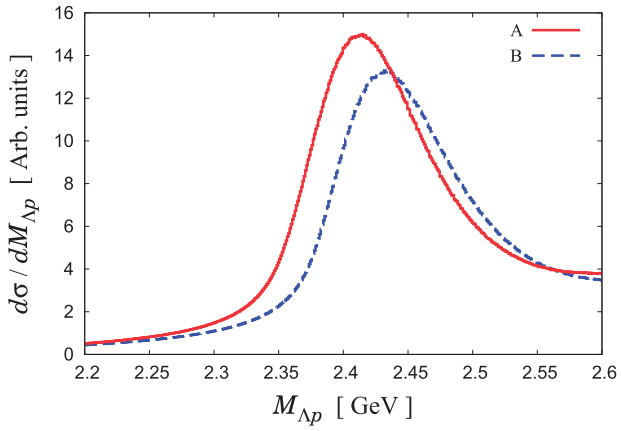

Fig. 7. Mass spectrum for the Λp invariant mass of the in-flight ^{3}He$(K^-, \Lambda p)n$ reaction with a constant T_2.

As for the dependence of the cross section on the cutoff of the form-factor employed in the $K^- p\Lambda$ vertex (15), we have found that Λ values in the range [0.7 GeV, 1.0 GeV] produce only quantitative differences in the corresponding mass spectra and angular distributions, while their shape is preserved. In particular, with the cutoff value $\Lambda = 1.0$ GeV the height of the mass spectrum becomes about 1.3 times larger than that with $\Lambda = 0.8$ GeV in both options A and B, and likewise the size of the spectra gets reduced by about 20% for a cutoff value of $\Lambda = 0.7$ GeV.

Let us discuss the difference between the results in options A and B. In option A (B), the peak height of the mass spectrum $d\sigma/dM_{\Lambda p}$ is about 110 μb/GeV (80 μb/GeV), and the peak position is about $M_{\Lambda p} = 2.37$ GeV (2.4 GeV). This difference in the peak structure is caused by the treatment of the kaon energies in the intermediate state and could be interpreted as a theoretical ambiguity in calculating the mass spectrum of this reaction in the present formulation.

In order to see the structure created by the underlying kinematic features of the amplitudes rather than by the uncorrelated $\Lambda(1405)p$ system, we take the amplitude T_2 as a constant:

$$T_2^{(K^- p \to K^- p)} = T_2^{(\bar{K}^0 n \to K^- p)} = \text{const.} \tag{33}$$

The result of the mass spectrum with this constant amplitude is plotted in Fig. 7. As one can see, even if we do not take into account the $\Lambda(1405)$ contribution, a peak appears in the $M_{\Lambda p}$ mass spectrum just above 2.4 GeV. This is due to the quasi-elastic scattering of the kaon in the first collision of the process. Namely, the intermediate kaon after the neutron emission at T_1 goes almost to its on mass shell, where the denominator of the propagator $1/[(p^{(\prime)0})^2 - \boldsymbol{p}^2 - m_K^2 + i m_K \Gamma_K]$ gets close to zero. Then, the peak position and its height are slightly different in options A and B. Since the energy $p^{(\prime)0}$ contains the kinetic energies of the nucleons with negative signs in option B, the denominator, $(p^{(\prime)0})^2 - \boldsymbol{p}^2 - m_K^2 + i m_K \Gamma_K$, gets close to zero for a larger value of $p'^0_\Lambda + p'^0_p$ in this option. This kinematic fact makes the peak in option B appear at a higher energy compared to that in A. We emphasize that this shift of the peak position makes a significant difference in the signal region. Actually, at the $\bar{K}NN$ threshold, the mass spectrum in Fig. 7 can be twice as large in option A as in option B. As a consequence, the uncorrelated $\Lambda(1405)p$ contribution, which can be calculated essentially by the product of the squared amplitude $|T_2|^2$ and the mass spectrum in Fig. 7 and whose peak position eventually appears around the $\bar{K}NN$ threshold, shows a non-negligible difference in both options.

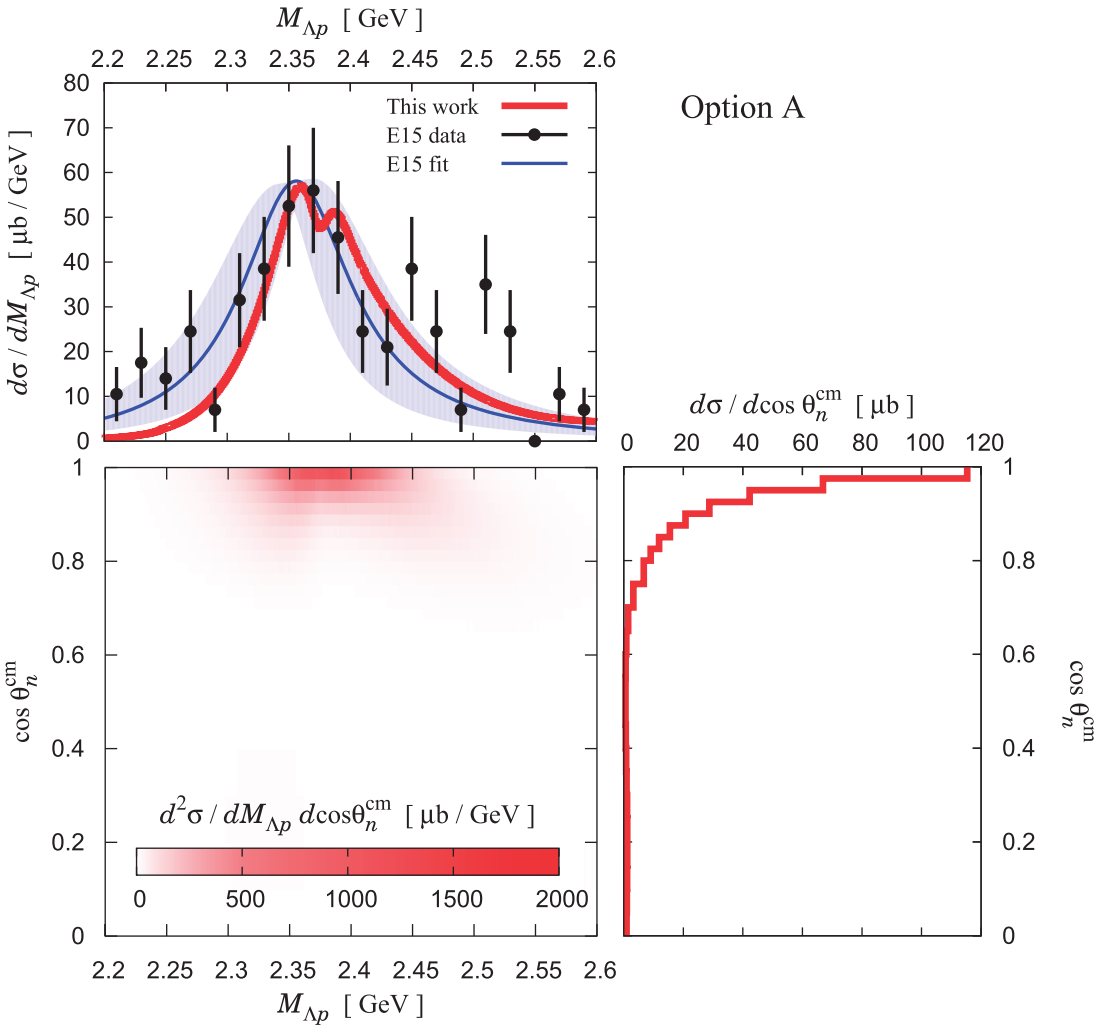

Fig. 8. Differential cross section for the in-flight ^{3}He$(K^-, \Lambda p)n$ reaction with generating the $\bar{K}NN$ quasi-bound state (see Fig. 2) in option A. The experimental (E15) data and its fit in the mass spectrum $d\sigma/dM_{\Lambda p}$ are taken from Ref. [29] and are shown in arbitrary units.

The other lesson that we learn from this exercise is that the peaks in Fig. 7 are shifted upwards by about 30 MeV with respect to those in Figs. 5 and 6. This reflects the fact that the excitation of the $\Lambda(1405)$ in Figs. 5 and 6 puts strength to the left of the quasi-elastic kaon peak, which makes it appear at lower energies merged with the signal of the uncorrelated $\Lambda(1405)p$ pair.

3.2. *Generating a $\bar{K}NN$ quasi-bound state*

In the previous subsection we showed that the experimental signal observed in the in-flight ^{3}He$(K^-, \Lambda p)n$ reaction at J-PARC [29] is definitely not the uncorrelated $\Lambda(1405)p$ state. Here we consider the case that a $\bar{K}NN$ quasi-bound state is generated after the first kaon scattering T_1, as formulated in Sect. 2.3. The numerical results are shown in Figs. 8 and 9.

An important thing to be noted is that the peak structure in our mass spectrum, regardless of option A or B, is consistent with the experimental results. In particular, we can reproduce qualitatively well the behavior of the tail of the peak below the K^-pp threshold, say at $M_{\Lambda p} = 2.3$ GeV. We also note

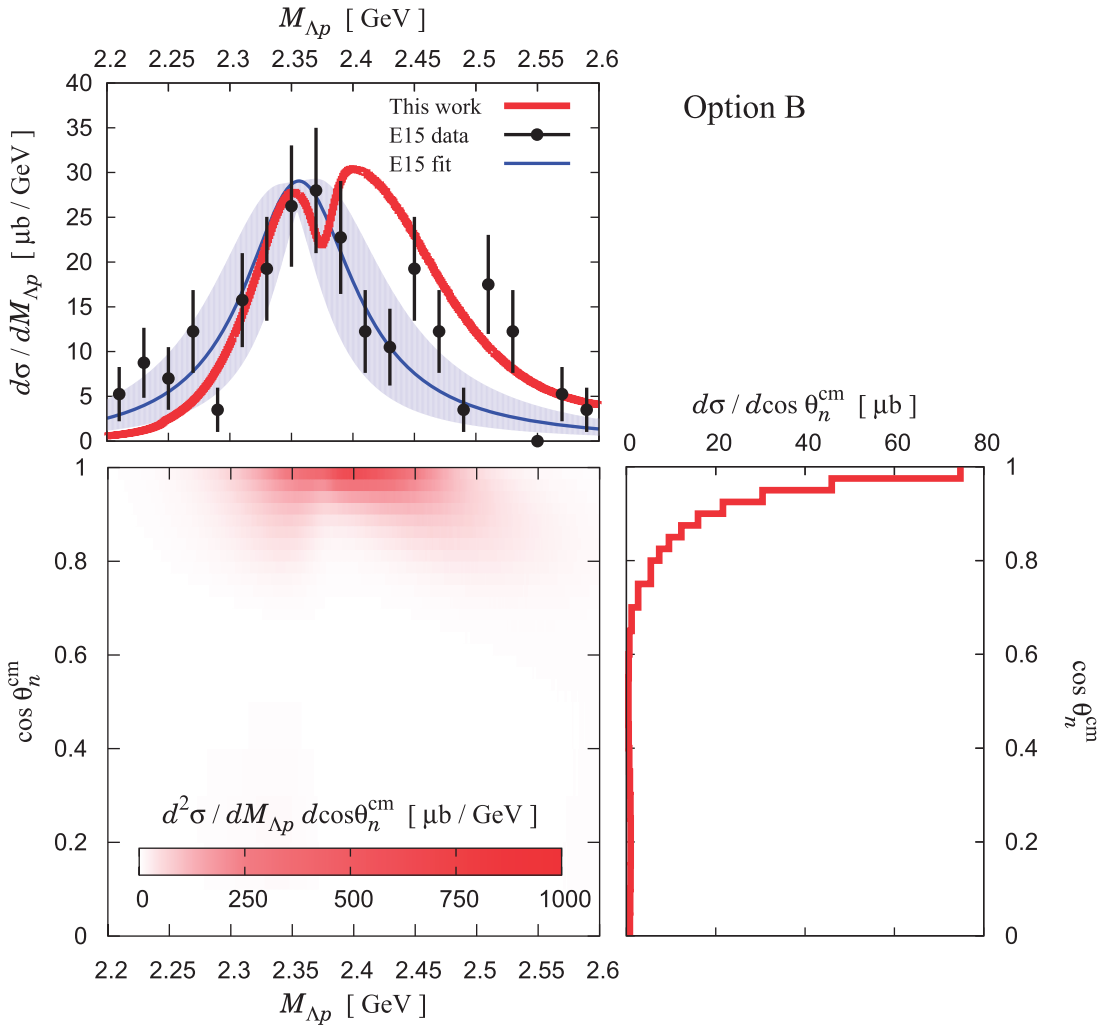

Fig. 9. The same as Fig. 8 for the kinematic option B.

that the width of our peak is similar to that in the experiment. Therefore, our mass spectrum supports the explanation that the peak structure observed in the experiment of Ref. [29] is indeed a signal of the $\bar{K}NN$ quasi-bound state.

Besides, interestingly, we observe a two-peak structure of the mass spectrum around the $\bar{K}NN$ threshold from the figures in both options A and B. The peak just below the $\bar{K}NN$ threshold corresponds to the $\bar{K}NN$ quasi-bound state, while the second peak just above the $\bar{K}NN$ threshold comes from the quasi-elastic scattering of the kaon, as seen in Fig. 7. Note that, since the mass spectrum is essentially a product of the mass spectrum in Fig. 7 and the square of the multiple scattering amplitude, $|T^{\rm FCA}|^2$, the obtained mass spectrum has the peak associated to that of $|T^{\rm FCA}|^2$ and another peak corresponding to that of the quasi-elastic kaon scattering, which is shifted to slightly lower energies by the effect of the energy dependence of $|T^{\rm FCA}|^2$ above its peak.

We emphasize that we cannot generate such a two-peak structure when we consider the case of the uncorrelated $\Lambda(1405)p$ system in the previous subsection. In principle, we would always have a possibility of having such a two-peak structure even in the uncorrelated $\Lambda(1405)p$ system: one associated with the quasi-elastic scattering of the kaon, i.e., the first intermediate antikaon practically

on-shell, and another structure linked with the "$\Lambda(1405)$ signal" of T_2. However, the location of these structures and their particular shapes in the uncorrelated $\Lambda(1405)p$ case make them merge into just one broader peak.

In contrast, for the case of the $\bar{K}NN$ quasi-bound state the locations of the peaks from the two origins are separated enough such that a two-peak structure remains. The facts that the spectrum in Fig. 7 falls fast to the left, while the dominant K^-pp component ($T_{11}^{\rm FCA} + T_{41}^{\rm FCA}$) in Fig. 4 falls fast to the right, also help in creating a dip in between the two peaks. This discussion indicates that, if such a two-peak structure was observed in experiments, it could be strong evidence that there should be a certain state originating from a dynamical factor, such as a $\bar{K}NN$ bound state, in addition to the quasi-elastic scattering of the kaon.

Note that the peak height of the mass spectrum in the case of the $\bar{K}NN$ bound state becomes about half of that of the uncorrelated $\Lambda(1405)p$ case. This is due to the combination of the structure tied to quasi-elastic kaon scattering in the first collision, shown in Fig. 7, with that of the scattering amplitude, which is either T_2, in the uncorrelated $\Lambda(1405)p$ case, or $T^{\rm FCA}$, in the $\bar{K}NN$ case. Hence, the peak produced by the T_2 or $T^{\rm FCA}$ amplitude will be multiplied by the quasi-elastic kaon scattering structure of Fig. 7. Actually, although the peak heights of T_2 and $T^{\rm FCA}$ are similar, their peak positions are displaced energetically, and this fact produces a drastic effect in the final value of the corresponding spectrum. Indeed, the peak of T_2 for the uncorrelated $\Lambda(1405)p$ case appears, due to some intrinsic momentum of the generated $\Lambda(1405)$, at invariant $M_{\Lambda p}$ masses above the $\bar{K}NN$ threshold and close to 2.4 GeV, which is the position of the kinematical peak associated to quasi-elastic scattering, hence producing an enhanced effect in the resulting mass spectrum. This is opposite in the correlated case producing the $\bar{K}NN$ bound state, since the $T^{\rm FCA}$ amplitude peaks around 2.35 GeV, a region where the strength of the kaon quasi-elastic structure has fallen down appreciably with respect to its peak. This explains why the mass spectrum obtained in the case of the $\bar{K}NN$ bound state becomes half of that for the uncorrelated $\Lambda(1405)p$ case.

In Figs. 8 and 9, we also plot the angular distribution of the cross section $d\sigma/d\cos\theta_n^{\rm cm}$, as well as the double differential cross section $d^2\sigma/dM_{\Lambda p}d\cos\theta_n^{\rm cm}$. Again there is no significant contribution in the region $\cos\theta_n^{\rm cm} < 0$. From these results, we can see that the structure at the $\bar{K}NN$ threshold is generated dominantly in the condition of forward neutron scattering. The reason is the same as that discussed in the previous subsection. In addition, we may observe two bands in the $d^2\sigma/dM_{\Lambda p}d\cos\theta_n^{\rm cm}$ plot of the figures, although their strength is weak; one goes from $M_{\Lambda p} \approx 2.35$ GeV at $\cos\theta_n^{\rm cm} = 1$ to the lower direction, and the other goes from the $\bar{K}NN$ threshold at $\cos\theta_n^{\rm cm} = 1$ to the lower-right direction. Actually, the former is the signal of the $\bar{K}NN$ quasi-bound state, and the latter is the contribution from the quasi-elastic scattering of the kaon.

Similarly to what we find in the uncorrelated $\Lambda(1405)p$ case, the use of different cutoff values affects only the size of the mass spectrum and the angular distribution of the $\bar{K}NN$ bound state signal. More specifically, using a cutoff value of $\Lambda = 1.0$GeV (0.7 GeV) gives rise to a mass spectrum that is about 1.3 times higher (1.2 times lower) than that with $\Lambda = 0.8$ GeV in both options A and B.

Finally, we compare the results of the mass spectrum employing options A and B in Fig. 10. As one can see, the strength of the peak is different in the two options, although their distributions become similar at the tails. In fact, the total cross section, calculated by integrating the mass spectrum $d\sigma/dM_{\Lambda p}$ with respect to the invariant mass $M_{\Lambda p}$, gives 7.6 μb for option A and 5.6 μb for option B. This difference in the strength can be explained by the results displayed in Fig. 7: the different location of the quasi-elastic kaon scattering peak produces a larger strength for option A than for option B.

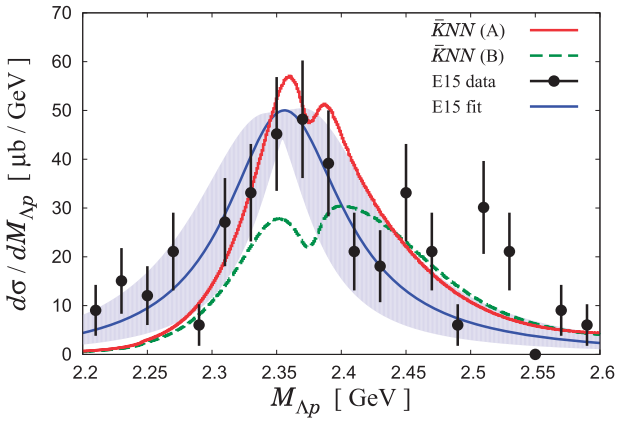

Fig. 10. Mass spectrum for the Λp invariant mass of the in-flight ^{3}He$(K^-, \Lambda p)n$ reaction. The E15 fit is scaled to reproduce the experimental value 7 μb [29].

In Fig. 10 we also plot the J-PARC E15 data and its fit, which is scaled to reproduce the empirical value of 7 μb [29]. We find that the absolute value of our mass spectrum is qualitatively consistent with the experimental one.[7]

4. Conclusion

We have studied the reaction ^{3}He$(K^-, \Lambda p)n$ measured recently in the J-PARC E15 experiment for a kaon beam of 1 GeV/c. This momentum is suited to producing secondary kaons nearly stopped when the neutrons go fast and forward in the laboratory system, which is guaranteed by a form factor that suppresses high momentum kaons in the intermediate state and $K^-n \to K^-n$ or $K^-p \to \bar{K}^0n$ cross sections that peak at backward kaon angles in the center of mass frame.

We have concentrated our study on mechanisms that involve the participation of the three nucleons in ^{3}He, allowing us to compare our results with the part of the experimental spectrum where there are no spectator nucleons. Our approach relies on a first collision of the K^- with a nucleon in ^{3}He, leading to the production of a slow $\bar{K}$ that is absorbed by the remaining NN pair. However, before the absorption takes place, the kaon is allowed to interact repeatedly with this pair of nucleons, hence providing a source of binding for the $\bar{K}NN$ system.

Technically, we employ a fully antisymmetrized ^{3}He wave function, which leads to many different combinations of first and second scattering processes, and we use Jacobi coordinates to describe the ^{3}He system. The $\bar{K}N$ interaction around threshold is obtained within a chiral unitary approach, and the interaction of the kaon with the two nucleons is treated in terms of the fixed center approximation to the Faddeev equation, which has proved to be enough to deal with this problem.

The results that we obtain are interesting. We observe that the Λp invariant mass distribution is clearly shifted to higher energies compared to experiment when the interaction of the slow kaon with the remaining two nucleons is not taken into account. The situation changes drastically when this interaction is considered, allowing for the formation of a $\bar{K}NN$ quasi-bound state, and producing a spectrum that reproduces the shape, position, and width of the experimental distribution. The total cross section obtained is also in good agreement with experiment within uncertainties.

[7] Note that one can only aim at a qualitative comparison since the J-PARC E15 experiment has not performed acceptance corrections so far.

A novel aspect of our approach is the presence of a two-peak structure in the Λp invariant mass spectrum, for which we provide a justification in terms of a quasi-elastic peak for $\bar{K}$ production in the first collision of the reaction and a peak associated to the production of the $\bar{K}NN$ bound state that decays into Λp. The present data, which have large error bars, do not permit us to infer this behavior. It will be interesting to see what the coming update of the experiment, with larger statistics, provides.

In any case, from the analysis of this experiment and comparison with the data, we can claim that the peak seen is indeed tied to the production of a quasi-bound $\bar{K}NN$ state, with properties very similar to those obtained in the work of Ref. [21] and to the average of other theoretical works.

Acknowledgements

The authors greatly acknowledge Y. Sada, T. Yamaga, F. Sakuma, J. Zmeskal, and M. Iwasaki for discussions on the data of the J-PARC E15 experiment. We acknowledge support by the Open Partnership Joint Projects of JSPS Bilateral Joint Research Projects. This work is partly supported by Grants-in-Aid for Scientific Research from MEXT and JSPS (No. 15K17649 and No. 15J06538), the Spanish Ministerio de Economia y Competitividad under the project MDM-2014-0369 of ICCUB and, with additional FEDER funds, under the contracts FIS2011-28853-C02-01 and FIS2014-54762-P, by the Generalitat Valenciana in the program Prometeo II, 2014/068, by the Generalitat de Catalunya contract 2014SGR-401, and by the Spanish Excellence Network on Hadronic Physics FIS2014-57026-REDT.

Funding

Open Access funding: SCOAP[3].

Appendix A. The wave function of ^{3}He

In this study, we evaluate the wave function of the ^{3}He nucleus with the harmonic oscillator potential governed by the following Hamiltonian:

$$\hat{H} = \sum_{i=1}^{3} \frac{\hat{\boldsymbol{p}}_i^2}{2m_i} + \sum_{i<j} \frac{k}{2} |\boldsymbol{r}_i - \boldsymbol{r}_j|^2, \tag{A.1}$$

where $\hat{\boldsymbol{p}}_i$ and $\boldsymbol{r}_i$ are the momentum operator and coordinate for the ith nucleon, respectively, and k is the spring constant taken as a parameter of the system. The mass of the nucleon is fixed as $m_1 = m_2 = m_3 = m_N$.

In order to separate the center-of-mass motion, we introduce the Jacobi coordinates

$$\begin{aligned} \boldsymbol{R} &\equiv \frac{m_1\boldsymbol{r}_1 + m_2\boldsymbol{r}_2 + m_3\boldsymbol{r}_3}{m_1 + m_2 + m_3} = \frac{\boldsymbol{r}_1 + \boldsymbol{r}_2 + \boldsymbol{r}_3}{3}, \\ \boldsymbol{\lambda} &\equiv \boldsymbol{r}_1 - \frac{m_2\boldsymbol{r}_2 + m_3\boldsymbol{r}_3}{m_2 + m_3} = \boldsymbol{r}_1 - \frac{\boldsymbol{r}_2 + \boldsymbol{r}_3}{2}, \quad \boldsymbol{\rho} \equiv \boldsymbol{r}_3 - \boldsymbol{r}_2, \end{aligned} \tag{A.2}$$

and their conjugate momenta

$$\begin{aligned} \hat{\boldsymbol{P}} &\equiv \hat{\boldsymbol{p}}_1 + \hat{\boldsymbol{p}}_2 + \hat{\boldsymbol{p}}_3, \\ \hat{\boldsymbol{p}}_\lambda &\equiv \frac{(m_2 + m_3)\hat{\boldsymbol{p}}_1 - m_1(\hat{\boldsymbol{p}}_2 + \hat{\boldsymbol{p}}_3)}{m_1 + m_2 + m_3} = \frac{2\hat{\boldsymbol{p}}_1 - \hat{\boldsymbol{p}}_2 - \hat{\boldsymbol{p}}_3}{3}, \quad \hat{\boldsymbol{p}}_\rho \equiv \frac{m_2\hat{\boldsymbol{p}}_3 - m_3\hat{\boldsymbol{p}}_2}{m_2 + m_3} = \frac{\hat{\boldsymbol{p}}_3 - \hat{\boldsymbol{p}}_2}{2}, \end{aligned} \tag{A.3}$$

respectively. With these Jacobi coordinates, we can rewrite the kinetic part of the Hamiltonian, regardless of values of the masses, as

$$\sum_{i=1}^{3} \frac{\hat{\boldsymbol{p}}_i^2}{2m_i} = \frac{\hat{\boldsymbol{P}}^2}{2M} + \frac{\hat{\boldsymbol{p}}_\lambda^2}{2m_\lambda} + \frac{\hat{\boldsymbol{p}}_\rho^2}{2m_\rho} \tag{A.4}$$

where

$$M \equiv m_1 + m_2 + m_3 = 3m_N,$$
$$m_\lambda \equiv \frac{m_1(m_2+m_3)}{M} = \frac{2}{3}m_N, \quad m_\rho \equiv \frac{m_2 m_3}{m_2+m_3} = \frac{1}{2}m_N. \tag{A.5}$$

On the other hand, in the potential term the λ and ρ modes decouple when $m_2 = m_3$, which is the case for ^{3}He, and its expression is

$$\sum_{i<j} \frac{k}{2}|\boldsymbol{r}_i - \boldsymbol{r}_j|^2 = \frac{1}{2}m_\lambda \omega_\lambda^2 \boldsymbol{\lambda}^2 + \frac{1}{2}m_\rho \omega_\rho^2 \boldsymbol{\rho}^2, \tag{A.6}$$

where the oscillator frequency is defined as

$$\omega_\lambda \equiv \left(\frac{2k}{m_\lambda}\right)^{1/2} = \left(\frac{3k}{m_N}\right)^{1/2}, \quad \omega_\rho \equiv \left(\frac{3k}{2m_\rho}\right)^{1/2} = \left(\frac{3k}{m_N}\right)^{1/2}. \tag{A.7}$$

As a consequence, the Hamiltonian can be rewritten as

$$\hat{H} = \frac{\hat{\boldsymbol{P}}^2}{2M} + \frac{\hat{\boldsymbol{p}}_\lambda^2}{2m_\lambda} + \frac{\hat{\boldsymbol{p}}_\rho^2}{2m_\rho} + \frac{1}{2}m_\lambda \omega_\lambda^2 \boldsymbol{\lambda}^2 + \frac{1}{2}m_\rho \omega_\rho^2 \boldsymbol{\rho}^2. \tag{A.8}$$

Now let us omit the center-of-mass motion and evaluate the wave function in terms of the λ and ρ modes. For the nucleons in ^{3}He, we assume that all of them are in the s-wave state and neglect contributions from higher partial waves such as the d wave, which are known to be small. In this condition, the wave function is expressed as the product of harmonic oscillator wave functions for the λ and ρ modes, both in the ground state:

$$\Psi(\lambda,\rho) = \left(\frac{m_\lambda \omega_\lambda}{\pi}\right)^{3/4} \exp\left(-\frac{1}{2}m_\lambda \omega_\lambda \lambda^2\right) \times \left(\frac{m_\rho \omega_\rho}{\pi}\right)^{3/4} \exp\left(-\frac{1}{2}m_\rho \omega_\rho \rho^2\right), \tag{A.9}$$

with $\lambda \equiv |\boldsymbol{\lambda}|$ and $\rho \equiv |\boldsymbol{\rho}|^2$. The normalization of the wave function is

$$\int d^3\lambda \int d^3\rho \, |\Psi(\lambda,\rho)|^2 = 1. \tag{A.10}$$

From the wave function, we can calculate the mean squared radius of the ^{3}He nucleus as the expectation value of r_i^2 for the ith nucleon measured from the center of mass. Namely,

$$\langle r_1^2 \rangle \equiv \int d^3\lambda \int d^3\rho \, |\boldsymbol{r}_1 - \boldsymbol{R}|^2 |\Psi(\lambda,\rho)|^2 = \int d^3\lambda \int d^3\rho \left|\frac{m_2+m_3}{M}\boldsymbol{\lambda}\right|^2 |\Psi(\lambda,\rho)|^2,$$
$$\langle r_2^2 \rangle \equiv \int d^3\lambda \int d^3\rho \, |\boldsymbol{r}_2 - \boldsymbol{R}|^2 |\Psi(\lambda,\rho)|^2 = \int d^3\lambda \int d^3\rho \left|-\frac{m_1}{M}\boldsymbol{\lambda} - \frac{m_3}{m_2+m_3}\boldsymbol{\rho}\right|^2 |\Psi(\lambda,\rho)|^2,$$
$$\langle r_3^2 \rangle \equiv \int d^3\lambda \int d^3\rho \, |\boldsymbol{r}_3 - \boldsymbol{R}|^2 |\Psi(\lambda,\rho)|^2 = \int d^3\lambda \int d^3\rho \left|-\frac{m_1}{M}\boldsymbol{\lambda} + \frac{m_2}{m_2+m_3}\boldsymbol{\rho}\right|^2 |\Psi(\lambda,\rho)|^2. \tag{A.11}$$

A straightforward calculation gives

$$\langle r_1^2 \rangle = \left(\frac{m_2 + m_3}{M} \right)^2 \frac{3}{2m_\lambda \omega_\lambda} = \left(\frac{1}{3km_N} \right)^{1/2}, \tag{A.12}$$

$$\langle r_2^2 \rangle = \langle r_3^2 \rangle = \left(\frac{m_1}{M} \right)^2 \frac{3}{2m_\lambda \omega_\lambda} + \left(\frac{m_3}{m_2 + m_3} \right)^2 \frac{3}{2m_\rho \omega_\rho} = \left(\frac{1}{3km_N} \right)^{1/2}. \tag{A.13}$$

As expected, one obtains the same value of the mean squared radius for each nucleon with $m_1 = m_2 = m_3 = m_N$. Then the parameter k can be fixed with the empirical value of the mean squared radius of ^{3}He, $\langle r_i^2 \rangle = 3.2\ \mathrm{fm}^2$. The result is

$$k = \frac{1}{3\langle r_i^2 \rangle^2 m_N} \approx 1.3\ \mathrm{MeV/fm}^2. \tag{A.14}$$

In this study we use the ^{3}He wave function in momentum space to calculate the scattering amplitude. For the harmonic oscillator potential, we can easily evaluate the wave function in momentum space as

$$\tilde{\Psi}(p_\lambda, p_\rho) = \left(\frac{4\pi}{m_\lambda \omega_\lambda} \right)^{3/4} \exp\left(-\frac{p_\lambda^2}{2m_\lambda \omega_\lambda} \right) \times \left(\frac{4\pi}{m_\rho \omega_\rho} \right)^{3/4} \exp\left(-\frac{p_\rho^2}{2m_\rho \omega_\rho} \right), \tag{A.15}$$

where $p_\lambda \equiv |\boldsymbol{p}_\lambda|$ and $p_\rho \equiv |\boldsymbol{p}_\rho|$. This is related to the wave function in coordinate space as

$$\tilde{\Psi}(p_\lambda, p_\rho) = \int d^3\lambda\ \exp(-i\boldsymbol{p}_\lambda \boldsymbol{\lambda}) \int d^3\rho\ \exp(-i\boldsymbol{p}_\rho \boldsymbol{\rho}) \Psi(\lambda, \rho), \tag{A.16}$$

and its normalization is

$$\int \frac{d^3p_\lambda}{(2\pi)^3} \int \frac{d^3p_\rho}{(2\pi)^3} \left| \tilde{\Psi}(p_\lambda, p_\rho) \right|^2 = 1. \tag{A.17}$$

Finally, taking into account the antisymmetrization for the nucleons in ^{3}He, we express the full wave function of the ^{3}He nucleus as

$$\begin{aligned} \left| {}^3\mathrm{He}(\chi) \right\rangle = \frac{1}{\sqrt{6}} \tilde{\Psi}(p_\lambda, p_\rho) \big[& |n(p_1, \chi) p(p_2, \chi_\uparrow) p(p_3, \chi_\downarrow)\rangle - |n(p_1, \chi) p(p_3, \chi_\downarrow) p(p_2, \chi_\uparrow)\rangle \\ & - |p(p_2, \chi_\uparrow) n(p_1, \chi) p(p_3, \chi_\downarrow)\rangle + |p(p_3, \chi_\downarrow) n(p_1, \chi) p(p_2, \chi_\uparrow)\rangle \\ & + |p(p_2, \chi_\uparrow) p(p_3, \chi_\downarrow) n(p_1, \chi)\rangle - |p(p_3, \chi_\downarrow) p(p_2, \chi_\uparrow) n(p_1, \chi)\rangle \big], \end{aligned} \tag{A.18}$$

for the spinor of the ^{3}He, $\chi = \chi_\uparrow = (1, 0)^t$ or $\chi_\downarrow = (0, 1)^t$. In this study the spin direction of ^{3}He is taken to be the same as that of the neutron.

Appendix B. $K^- p \to \bar{K}^0 n$ and $K^- n \to K^- n$ scattering amplitudes at $k_{\mathrm{lab}} = 1\ \mathrm{GeV}/c$

In this appendix we formulate the $K^- p \to \bar{K}^0 n$ and $K^- n \to K^- n$ scattering amplitudes at $k_{\mathrm{lab}} = 1\ \mathrm{GeV}/c$, which are needed to emit the fast neutron in the final state of the $^3\mathrm{He}(K^-, \Lambda p)n$ reaction. In this study, we neglect the spin flip contribution and estimate the scattering amplitude $T_{\bar{K}N \to \bar{K}N}$

Table B1. Parameter sets for the $K^- p \to \bar{K}^0 n$ and $K^- n \to K^- n$ scattering amplitudes at $k_{\rm lab} = 1\,{\rm GeV}/c$ (all the parameters are given in units of mb/sr).

	$K^- p \to \bar{K}^0 n$	$K^- n \to K^- n$
c_0	0.57	0.94
c_1	−0.05	0.51
c_2	0.65	1.38
c_3	−0.42	—
c_4	0.76	—

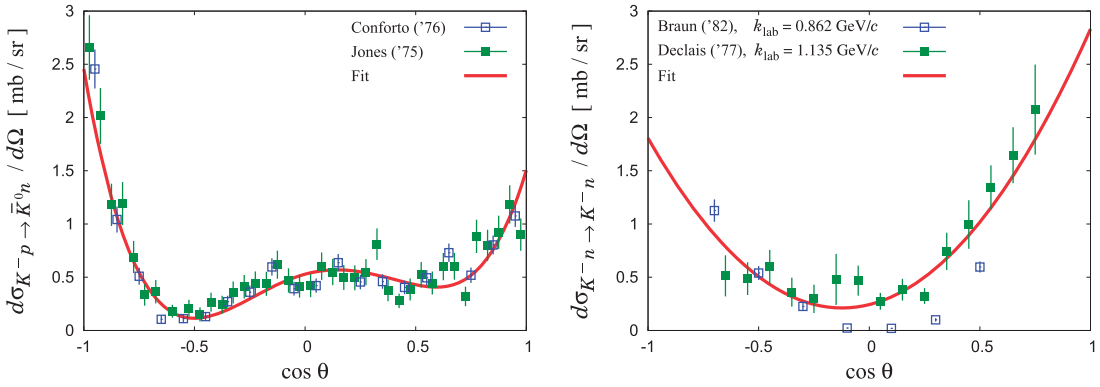

Fig. B.1. Differential cross sections of the $K^- p \to \bar{K}^0 n$ (left) and $K^- n \to K^- n$ (right) reactions, where θ is the angle of the emerging kaon versus the original one. The experimental data are taken from Refs. [41,42] at $k_{\rm lab} = 1\,{\rm GeV}/c$ for a proton target, and from Ref. [43] at $k_{\rm lab} = 1.138\,{\rm GeV}/c$ and from Ref. [44] at $k_{\rm lab} = 0.862\,{\rm GeV}/c$ for a neutron target.

of these reactions at $k_{\rm lab} = 1\,{\rm GeV}/c$ from the differential cross section $d\sigma_{\bar{K}N\to\bar{K}N}/d\Omega$ with the following formula:

$$T_{\bar{K}N\to\bar{K}N}(\cos\theta) = \frac{4\pi w_1}{m_N}\left(\frac{d\sigma_{\bar{K}N\to\bar{K}N}}{d\Omega}\right)^{1/2}, \tag{B.1}$$

where θ is the scattering angle for the kaon, $w_1 \equiv \left((p_{\bar{K}} + p_N)^2\right)^{1/2}$, and m_N is the nucleon mass. When we theoretically calculate the differential cross section, we always fix the initial kaon momentum as $k_{\rm lab} = 1\,{\rm GeV}/c$.

We parametrize the differential cross section $d\sigma_{\bar{K}N\to\bar{K}N}/d\Omega$ by the Legendre polynomials $P_l(x)$ as

$$\frac{d\sigma_{\bar{K}N\to\bar{K}N}}{d\Omega} = \sum_l c_l P_l(\cos\theta), \tag{B.2}$$

with constants c_l that are fixed to reproduce the experimental data. For the proton target reaction, we have many experimental data points for the differential cross section at $k_{\rm lab} = 1\,{\rm GeV}/c$ [41,42], so we take the polynomials up to $l = 4$. From the best fit we obtain the parameters c_l listed in Table B1. For the neutron target reaction, on the other hand, only the data at $k_{\rm lab} = 1.138\,{\rm GeV}/c$ [43] and at $k_{\rm lab} = 0.862\,{\rm GeV}/c$ [44] are available, so we take the polynomials up to $l = 2$ and make a rough fit to the cross sections at these momenta. As a result, we obtain the parameters in Table B1. For both

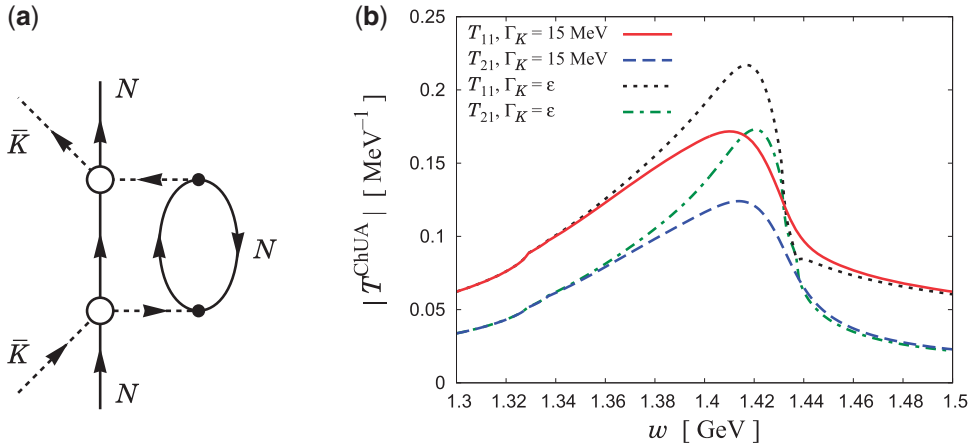

Fig. C.1. (a) Feynman diagram corresponding to the kaon absorption by two nucleons. The unspecified solid and dashed lines represent baryons and mesons, respectively. (b) Absolute values of the scattering amplitudes in the chiral unitary approach for the $K^-p \to K^-p$ (T_{11}) and $\bar{K}^0n \to K^-p$ (T_{21}) reactions with the kaon absorption width $\Gamma_K = 15$ MeV. For comparison we also show the amplitudes with zero absorption width, $\Gamma_K = \epsilon$.

reactions, the fitted differential cross sections are shown in Fig. B.1 together with the experimental data.

Appendix C. $\bar{K}N \to \bar{K}N$ scattering amplitude around threshold

In this appendix we briefly introduce the $\bar{K}N \to \bar{K}N$ scattering amplitude around threshold, which appears in the secondary scattering of the $^3\mathrm{He}(K^-, \Lambda p)n$ reaction and in the multiple scattering of the $\bar{K}NN$ system. For this amplitude we employ the so-called chiral unitary approach [1,2,4,5], modified to take into account the kaon absorption by two nucleons in the $\bar{K}NN$ system in a simple way. In this study we introduce ten meson–baryon channels: K^-p, $\bar{K}^0n$, $\pi^0\Lambda$, $\pi^0\Sigma^0$, $\pi^+\Sigma^-$, $\pi^-\Sigma^+$, $\eta\Lambda$, $\eta\Sigma^0$, $K^0\Xi^0$, and $K^+\Xi^-$. Since we are interested in the amplitude around the $\bar{K}N$ threshold, we consider its s-wave part only.

In the chiral unitary approach, the $\bar{K}N \to \bar{K}N$ scattering amplitude T_{ij}^{ChUA}, where i and j are channel indices, is the solution of the coupled-channels Lippmann–Schwinger equation in an algebraic form:

$$T_{ij}^{\mathrm{ChUA}}(w) = V_{ij}(w) + \sum_k V_{jk}(w) G_k(w) T_{kj}^{\mathrm{ChUA}}(w) = \sum_k [1 - VG]^{-1}{}_{ik} V_{kj}. \tag{C.1}$$

Here, w is the center-of-mass energy, V_{ij} is the interaction kernel taken from chiral perturbation theory, and G_k is the meson–baryon loop function. In this study the interaction kernel V_{ij} is fixed to be the leading order term of chiral perturbation theory for the s-wave meson-baryon scattering, i.e., the Weinberg–Tomozawa term, whose expression is given in Ref. [5]. We note that in this scheme we can effectively take into account the kaon absorption by two nucleons, whose diagram is shown in Fig. C.1(a), in a simple way by just adding the imaginary part of that diagram by means of an

empirical width Γ_K in the kaon propagator. The loop function is then evaluated with the cutoff scheme as

$$G_i(w) = \int_{q<q_{\max}} \frac{d^3q}{(2\pi)^3} \frac{M_i}{2\omega_i(\boldsymbol{q})E_i(\boldsymbol{q})} \frac{1}{w-\omega_i(\boldsymbol{q})-E_i(\boldsymbol{q})+i\Gamma_i}, \tag{C.2}$$

$$\omega_i(\boldsymbol{q}) \equiv \left(\boldsymbol{q}^2+m_i^2\right)^{1/2}, \quad E_i(\boldsymbol{q}) \equiv \left(\boldsymbol{q}^2+M_i^2\right)^{1/2}, \quad \Gamma_i = \begin{cases} \Gamma_K & \text{for } i = K^-p, \bar{K}^0n, \\ \epsilon & \text{for other channels,} \end{cases} \tag{C.3}$$

where $q_{\max}$ is the cutoff, M_i and m_i are the baryon and meson masses in channel i, respectively, Γ_K is the kaon absorption width by two nucleons, and ϵ is an infinitesimal positive value.

In this study we take the cutoff as $q_{\max} = 630$ MeV [2], and the kaon absorption width is fixed to be $\Gamma_K = 15$ MeV so as to reproduce the kaon absorption width of the $\bar{K}NN$ bound state in the fixed center approximation [21] (see Appendix D). With these values, we can calculate the $\bar{K}N \to \bar{K}N$ scattering amplitude as plotted in Fig. C.1(b). As one can see from the figure, the introduction of the absorption width $\Gamma_K = 15$ MeV shifts the peak position for the $\Lambda(1405)$ resonance ~ 1.4 GeV only slightly, but the width of the $\Lambda(1405)$ peak grows to ~ 50 MeV. Actually, for this amplitude with $\Gamma_K = 15$ MeV, we find a resonance pole corresponding to the peak in Fig. C.1(b) at $w = 1428 - 26i$ MeV in the complex energy plane, which was $1427 - 19i$ MeV for $\Gamma_K = \epsilon$.

Appendix D. Kaon multiple scattering amplitude in the fixed center approximation

In this appendix we formulate the kaon multiple scattering amplitude for the $\bar{K}NN$ three-body state. In this study we employ the so-called fixed center approximation to the Faddeev equation [17,21]. For the sake of simplicity in the calculation, isospin symmetric masses are employed in the calculation of the $\bar{K}NN$ multiple scattering amplitude.

Since we are interested in the K^-pp states and others coupling to this, we consider six channels for the $\bar{K}NN$ three-body state: K^-pp, $\bar{K}^0np$, $\bar{K}^0pn$, ppK^-, $np\bar{K}^0$, and $pn\bar{K}^0$, which are labeled by indices i and j in the above order. We note that we distinguish the ordering of the kaon and two nucleons so as to specify the nucleon with which the kaon interacts first and last. For instance, in the channel K^-pn (pnK^-) in the initial state, K^- interacts first with the proton on the left (neutron on the right). With this, we can divide the multiple scattering processes into an even number and an odd number of scatterings, which makes the formulation of the multiple scattering easier.

We note that pion exchange between two nucleons is neglected in the diagrams that build the $T^{\rm FCA}$ amplitude; see Fig. 3. In fact, these pion exchange contributions may either appear in the last of the multiple scatterings or correspond to exchanges in intermediate states. In the first case, the pion exchange is accompanied by the $\bar{K}N \to \pi\Lambda$ amplitude and by the absorption of the pion via the πNN vertex. Since the amplitude $\bar{K}N \to \pi\Lambda$ has isospin $I = 1$, the contribution from the first case should be small. In the second case, the pion exchange is accompanied by the $\pi N \to \pi N$ amplitude, but this contribution in the intermediate states has been found to be small in Ref. [45].

Here, in order to grasp the structure of the multiple scattering in the fixed center approximation, we first consider the $K^-pp \to K^-pp$ amplitude $T_{11}^{\rm FCA}$, which is shown diagrammatically in Fig. D.1. This can be expressed in the following equation:

$$T_{11}^{\rm FCA} = t_1 + t_1G_0T_{41}^{\rm FCA} + t_2G_0T_{51}^{\rm FCA}, \tag{D.1}$$

where t is the $\bar{K}N \to \bar{K}N$ scattering amplitude and G_0 is the kaon propagator, both of which are functions of the total energy of the $\bar{K}NN$ system only, i.e., the Λp invariant mass. The $\bar{K}N \to \bar{K}N$

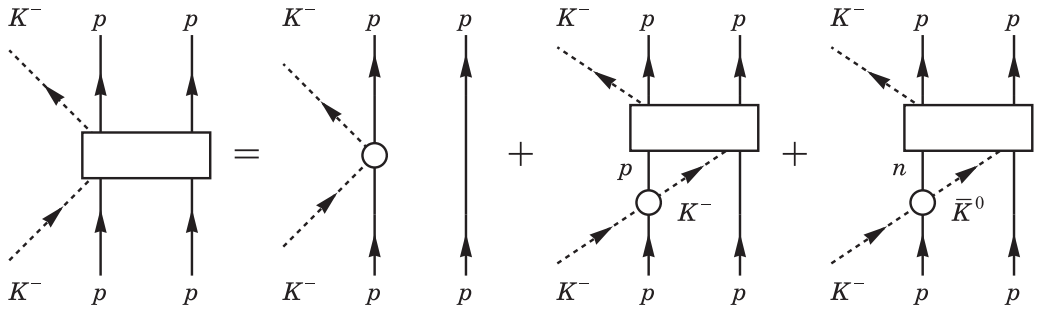

Fig. D.1. Feynman diagrams for the kaon multiple scattering of the process $K^- pp \to K^- pp$. The open rectangles indicate the $\bar{K}NN$ multiple scattering amplitude and the circles represent the one for $\bar{K}N \to \bar{K}N$.

scattering amplitude is fixed in the chiral unitary approach

$$t_1(M_{\Lambda p}) = T^{\rm ChUA}_{K^- p \to K^- p}(w_{\rm FCA}), \quad t_2(M_{\Lambda p}) = T^{\rm ChUA}_{K^- p \to \bar{K}^0 n}(w_{\rm FCA}) = T^{\rm ChUA}_{\bar{K}^0 n \to K^- p}(w_{\rm FCA}), \tag{D.2}$$

where the argument $w_{\rm FCA}$ is [17]

$$w_{\rm FCA}(M_{\Lambda p}) \equiv \left(\frac{M_{\Lambda p}^2 + m_K^2 - 2m_N^2}{2} \right)^{1/2}. \tag{D.3}$$

The kaon propagator G_0 is evaluated as

$$G_0(M_{\Lambda p}) \equiv \int \frac{d^3q}{(2\pi)^3} \frac{F_{NN}(\boldsymbol{q})}{q^0_{\rm FCA}(M_{\Lambda p})^2 - \omega_K(\boldsymbol{q})^2 + i m_K \Gamma_K}, \tag{D.4}$$

$$q^0_{\rm FCA}(M_{\Lambda p}) \equiv \frac{M_{\Lambda p}^2 + m_K^2 - (2m_N)^2}{2M_{\Lambda p}}, \tag{D.5}$$

with the kaon energy $\omega_K(\boldsymbol{q}) \equiv \left(\boldsymbol{q}^2 + m_K^2\right)^{1/2}$ and the form factor for the NN system,

$$F_{NN}(\boldsymbol{q}) \equiv \int d^3r \, \exp(i\boldsymbol{q}\boldsymbol{r}) |\varphi(r)|^2. \tag{D.6}$$

Here $\varphi(r)$ is the wave function for the NN system, for which we take the ρ mode of the ^{3}He wave function as (see Appendix A)

$$F_{NN}(\boldsymbol{q}) = \int d^3\rho \, \exp(i\boldsymbol{q}\boldsymbol{\rho}) \left(\frac{m_\rho \omega_\rho}{\pi} \right)^{3/2} \exp(-m_\rho \omega_\rho \rho^2) = \exp\left(-\frac{\boldsymbol{q}^2}{(4 m_\rho \omega_\rho)} \right), \tag{D.7}$$

with $m_\rho = m_N/2$ and ω_ρ in Eq. (A.7).[8]

In a similar manner we can express the multiple scattering amplitude $T^{\rm FCA}_{ij}$ with the tree-diagram contributions, containing only $\bar{K}N$ two-body amplitudes, and tree times further multiple scattering amplitudes. As a result, the multiple scattering amplitude $T^{\rm FCA}_{ij}$ is found to be a solution of the scattering equation

$$T^{\rm FCA}_{ij} = V^{\rm FCA}_{ij} + \sum_{k=1}^{6} \tilde{V}^{\rm FCA}_{ik} G_0 T^{\rm FCA}_{kj} = \sum_{k=1}^{6} \left[1 - \tilde{V}^{\rm FCA} G_0 \right]^{-1}_{ik} V^{\rm FCA}_{kj}, \tag{D.8}$$

[8] For the ^{3}He wave function, we use isospin symmetric nucleon mass m_N: $m_N = (m_p + m_n)/2$.

with

$$V^{\rm FCA} = \begin{pmatrix} t_1 & t_2 & 0 & 0 & 0 & 0 \\ t_2 & t_3 & 0 & 0 & 0 & 0 \\ 0 & 0 & t_4 & 0 & 0 & 0 \\ 0 & 0 & 0 & t_1 & 0 & t_2 \\ 0 & 0 & 0 & 0 & t_4 & 0 \\ 0 & 0 & 0 & t_2 & 0 & t_3 \end{pmatrix}, \quad \tilde{V}^{\rm FCA} = \begin{pmatrix} 0 & 0 & 0 & t_1 & t_2 & 0 \\ 0 & 0 & 0 & t_2 & t_3 & 0 \\ 0 & 0 & 0 & 0 & 0 & t_4 \\ t_1 & 0 & t_2 & 0 & 0 & 0 \\ 0 & t_4 & 0 & 0 & 0 & 0 \\ t_2 & 0 & t_3 & 0 & 0 & 0 \end{pmatrix}. \tag{D.9}$$

Here t_3 and t_4 are

$$t_3(M_{\Lambda p}) = T^{\rm ChUA}_{\bar{K}^0 n \to \bar{K}^0 n}(w_{\rm FCA}), \quad t_4(M_{\Lambda p}) = T^{\rm ChUA}_{\bar{K}^0 p \to \bar{K}^0 p}(w_{\rm FCA}), \tag{D.10}$$

and t_1 and t_2 have been defined in Eq. (D.2). We note that the multiple scattering amplitude $T^{\rm FCA}$ depends only on the invariant mass $M_{\Lambda p}$.

With this formulation, we can plot the multiple scattering amplitude as in Fig. 4. The kaon absorption width Γ_K in G_0 is fixed as $\Gamma_K = 15\,\text{MeV}$, so that the amplitude $T^{\rm FCA}_{11} + T^{\rm FCA}_{41}$ reproduces the width of the $\bar{K}NN$ bound-state signal in the fixed center approximation [21]. For this amplitude in the fixed center approximation, we find a pole at $M_{\Lambda p} = 2354 - 36i\,\text{MeV}$ in the complex plane of the invariant mass $M_{\Lambda p}$, corresponding to the peak in Fig. 3.

References

[1] N. Kaiser, P. B. Siegel, and W. Weise, Nucl. Phys. A **594**, 325 (1995).
[2] E. Oset and A. Ramos, Nucl. Phys. A **635**, 99 (1998).
[3] Y. Kamiya, K. Miyahara, S. Ohnishi, Y. Ikeda, T. Hyodo, E. Oset, and W. Weise, Nucl. Phys. A **954**, 41 (2016). [arXiv:1602.08852 [hep-ph]] [Search INSPIRE].
[4] J. A. Oller and U. G. Meissner, Phys. Lett. B **500**, 263 (2001).
[5] D. Jido, J. A. Oller, E. Oset, A. Ramos, and U. G. Meissner, Nucl. Phys. A **725**, 181 (2003).
[6] K. A. Olive et al. [Particle Data Group Collaboration], Chin. Phys. C **38**, 090001 (2014).
[7] U. G. Meissner and T. Hyodo, Review of Particle Physics. Available at http://pdg.lbl.gov/2015/reviews/rpp2015-rev-lam-1405-pole-struct.pdf, date last accessed December 6, 2016.
[8] Y. Akaishi and T. Yamazaki, Phys. Rev. C **65**, 044005 (2002).
[9] N. V. Shevchenko, A. Gal, and J. Mares, Phys. Rev. Lett. **98**, 082301 (2007).
[10] N. V. Shevchenko, A. Gal, J. Mares, and J. Revai, Phys. Rev. C **76**, 044004 (2007).
[11] Y. Ikeda and T. Sato, Phys. Rev. C **76**, 035203 (2007).
[12] Y. Ikeda and T. Sato, Phys. Rev. C **79**, 035201 (2009).
[13] Y. Ikeda, H. Kamano, and T. Sato, Prog. Theor. Phys. **124**, 533 (2010).
[14] A. Dote, T. Hyodo, and W. Weise, Nucl. Phys. A **804**, 197 (2008).
[15] A. Dote, T. Hyodo, and W. Weise, Phys. Rev. C **79**, 014003 (2009).
[16] S. Wycech and A. M. Green, Phys. Rev. C **79**, 014001 (2009).
[17] M. Bayar, J. Yamagata-Sekihara, and E. Oset, Phys. Rev. C **84**, 015209 (2011).
[18] N. Barnea, A. Gal, and E. Z. Liverts, Phys. Lett. B **712**, 132 (2012).
[19] A. Dote, T. Inoue, and T. Myo, Prog. Theor. Exp. Phys. **2015**, 043D02 (2015) [arXiv:1411.0348 [nucl-th]] [Search INSPIRE].
[20] A. Gal, Nucl. Phys. A **914**, 270 (2013).
[21] M. Bayar and E. Oset, Phys. Rev. C **88**, 044003 (2013).
[22] T. Uchino, T. Hyodo, and M. Oka, Nucl. Phys. A **868-869**, 53 (2011).
[23] A. Ramos, V. K. Magas, E. Oset, and H. Toki, Nucl. Phys. A **804**, 219 (2008).
[24] M. Agnello et al. [FINUDA Collaboration], Phys. Rev. Lett. **94**, 212303 (2005).
[25] T. Yamazaki et al., Phys. Rev. Lett. **104**, 132502 (2010).
[26] A. O. Tokiyasu et al. [LEPS Collaboration], Phys. Lett. B **728**, 616 (2014).

[27] Y. Ichikawa et al. [J-PARC E27 Collaboration], Prog. Theor. Exp. Phys. **2015**, 021D01 (2015) [arXiv:1411.6708 [nucl-ex]] [Search INSPIRE].
[28] T. Hashimoto et al. [J-PARC E15 Collaboration], Prog. Theor. Exp. Phys. **2015**, 061D01 (2015) [arXiv:1408.5637 [nucl-ex]] [Search INSPIRE].
[29] Y. Sada et al. [J-PARC E15 Collaboration], Prog. Theor. Exp. Phys. **2016**, 051D01 (2016) [arXiv:1601.06876 [nucl-ex]] [Search INSPIRE].
[30] J. M. M. Hall, W. Kamleh, D. B. Leinweber, B. J. Menadue, B. J. Owen, A. W. Thomas, and R. D. Young, Phys. Rev. Lett. **114**, 132002 (2015).
[31] T. Sekihara, T. Hyodo, and D. Jido, Prog. Theor. Exp. Phys. **2015**, 063D04 (2015) [arXiv:1411.2308 [hep-ph]] [Search INSPIRE].
[32] Y. Kamiya and T. Hyodo, Phys. Rev. C **93**, 035203 (2016).
[33] T. Sekihara, D. Jido, and Y. Kanada-En'yo, Phys. Rev. C **79**, 062201 (2009).
[34] T. Sekihara, J. Yamagata-Sekihara, D. Jido, and Y. Kanada-En'yo, Phys. Rev. C **86**, 065205 (2012).
[35] D. Jido, E. Oset, and T. Sekihara, Eur. Phys. J. A **42**, 257 (2009).
[36] D. Jido, E. Oset, and T. Sekihara, Eur. Phys. J. A **47**, 42 (2011).
[37] J. Yamagata-Sekihara, T. Sekihara, and D. Jido, Prog. Theor. Exp. Phys. **2013**, 043D02 (2013) [arXiv:1210.6108 [nucl-th]] [Search INSPIRE].
[38] D. Jido, E. Oset, and T. Sekihara, Eur. Phys. J. A **49**, 95 (2013).
[39] K. M. Watson, Phys. Rev. **89**, 575 (1953).
[40] K. Miyagawa and J. Haidenbauer, Phys. Rev. C **85**, 065201 (2012).
[41] M. Jones, R. Levi Setti, D. Merrill, and R. D. Tripp, Nucl. Phys. B **90**, 349 (1975).
[42] B. Conforto et al. [Rutherford-London Collaboration], Nucl. Phys. B **105**, 189 (1976).
[43] Y. Declais et al., CERN-77-16, CERN-YELLOW-77-16.
[44] O. Braun, V. Hepp, H. Strobele, W. Wittek, and P. Baillon, Nucl. Phys. B **203**, 349 (1982).
[45] S. S. Kamalov, E. Oset, and A. Ramos, Nucl. Phys. A **690**, 494 (2001).